Pflugers Arch - Eur J Physiol (2012) 463:625–633
DOI 10.1007/s00424-012-1082-2

SIGNALING AND CELL PHYSIOLOGY

Regulatory mechanisms underlying the modulation of GIRK1/GIRK4 heteromeric channels by P2Y receptors

Jie Wu · Wei-Guang Ding · Hiroshi Matsuura · Minoru Horie

Received: 17 October 2011 /Revised: 5 February 2012 /Accepted: 6 February 2012 /Published online: 24 February 2012

Abstract The muscarinic K^+ channel ($I_{K,ACh}$) is a hetero-tetramer composed of GIRK1 (Kir3.1) and GIRK4 (Kir3.4) subunits of a G protein-coupled inwardly rectifying channel, and plays an important role in mediating electrical responses to the vagal stimulation in the heart. $I_{K,ACh}$ displays biphasic changes (activation followed by inhibition) through the stimulation of the purinergic P2Y receptors, but the regulatory mechanism involved in these modulation of $I_{K,ACh}$ by P2Y receptors remains to be fully elucidated. Various P2Y receptor subtypes and GIRK1/GIRK4 (I_{GIRK}) were co-expressed in Chinese hamster ovary cells, and the effect of stimulation of P2Y receptor subtypes on I_{GIRK} were examined using the whole-cell patch-clamp method. Extracellular application of 10 μM ATP induced a transient activation of I_{GIRK} through the $P2Y_1$ receptor, which was completely abolished by pretreatment with pertussis toxin. ATP initially caused an additive transient increase in ACh-activated I_{GIRK} (via M_2 receptor), which was followed by subsequent inhibition. This inhibition of I_{GIRK} by ATP was attenuated by co-expression of regulator of G-protein signaling 2, or phosphatidylinositol-4-phosphate-5-kinase, or intracellular phosphatidylinositol 4,5-bisphosphate loading, but not by the exposure to protein kinase C inhibitors. $P2Y_4$ stimulation also persistently suppressed the ACh-activated I_{GIRK}. In addition, I_{GIRK} evoked by the stimulation of the $P2Y_4$ receptor exhibited a transient activation, but that evoked by the stimulation of $P2Y_2$ or $P2Y_{12}$ receptor showed a rather persistent activation. These results reveal (1) that $P2Y_1$ and $P2Y_4$ are primarily coupled to the G_q-phospholipase C-pathway, while being weakly linked to $G_{i/o}$, and (2) that $P2Y_2$ and $P2Y_{12}$ involve $G_{i/o}$ activation.

Keywords GIRK1/GIRK4 · P2Y receptors · I_{GIRK} · PIP_2 · Patch clamp · CHO

Abbreviations

ACh	Acetylcholine
$I_{K,ACh}$	Muscarinic K^+ channel
PLC	Phospholipase C
PKC	Protein kinase C
PIP_2	Phosphatidylinositol 4,5-bisphosphate
PTX	Pertussis toxin
PI4P-5K	Phosphatidylinositol-4-phosphate-5-kinase
CHO	Chinese hamster ovary
AC	Adenylyl cyclase
WT	Wild type
GFP	Green fluorescent protein
ATP	Adenosine triphosphate
UTP	Uridine triphosphate
RGS_2	Regulator of G-protein signaling 2
GIRK	G protein-activated inward rectifier K^+ channel

Jie Wu and Wei-Guang Ding have contributed equally to this work.

Electronic supplementary material The online version of this article (doi:10.1007/s00424-012-1082-2) contains supplementary material, which is available to authorized users.

J. Wu
Department of Pharmacology,
Medical School of Xi'an Jiaotong University,
Xi'an, Shaanxi 710061, People's Republic of China

J. Wu · W.-G. Ding · H. Matsuura (✉)
Department of Physiology, Shiga University of Medical Science,
Otsu, Shiga 520-2192, Japan
e-mail: matuurah@belle.shiga-med.ac.jp

J. Wu · M. Horie (✉)
Department of Cardiovascular and Respiratory Medicine,
Shiga University of Medical Science,
Otsu, Shiga 520-2192, Japan
e-mail: horie@belle.shiga-med.ac.jp

Introduction

The muscarinic K^+ channel ($I_{K,ACh}$) is a heterotetramer that comprises Kir3.1 and Kir3.4 subunits (encoded by GIRK1 and GIRK4, respectively) of G protein-coupled inwardly rectifying channel. $I_{K,ACh}$ plays an important role in mediating negative inotropic, chronotropic, and dromotropic responses to the vagal neurotransmitter acetylcholine (ACh) in the heart [20]. Previous reports indicate that adenosine 5′-triphosphate (ATP) produces dual effects on $I_{K,ACh}$: a transient activation followed by a persistent inhibition, in guinea pig atrial cells [13, 24, 44]. Like other neurotransmitters such as ACh [34, 35] and adenosine [21, 24], ATP activates the membrane receptors coupled to the $I_{K,ACh}$ channel proteins through a pertussis toxin (PTX) sensitive heterotetrameric G protein, thus leading to the dissociation of the heterotrimeric G-protein complex into its α and $\beta\gamma$ subunits that can interact with the channel and cause an increase in open-state probability of the channel [5, 24, 42]. Conversely, $I_{K,ACh}$ is persistently inhibited by ATP following the transient activation. Previous studies using guinea pig atrial cells [25, 44] demonstrated that the inhibition of $I_{K,ACh}$ by ATP is associated with activation of the P2Y receptors that are coupled to a PTX-insensitive G protein leading to activation of G_q-phospholipase C (PLC) signaling pathway. However, the modulatory mechanism underlying the inhibition of $I_{K,ACh}$ by P2Y receptor subtype stimulation has yet to be fully elucidated.

P2Y receptors belong to G protein-coupled P2 purinergic receptors that can be activated by purine or pyrimidine nucleotides. Eight P2Y receptor subtypes ($P2Y_{1,\ 2,\ 4,\ 6,\ 11,\ 12,\ 13}$ and $_{14}$) have been cloned from mammalian cells, and all of them are expressed in heart tissues and associated with the extracellular signaling pathway [3, 10, 30, 37]. Several studies have so far indicated that ATP elicits diverse functional responses in various types of tissues including cardiac cells [10, 26, 27]. However, the functional coupling correlates of the involved P2Y receptor subtypes in cardiac cells is still a topic of debate and remains difficult in native cell due to the restricted availability of subtype-selective ligands and/or blockers.

The present study was undertaken to further explore the inhibitory mechanism of $I_{K,ACh}$ using Chinese hamster ovary (CHO) cells heterologously co-expressed with GIRK1/GIRK4 and different P2Y receptor subtypes. The result reveals that stimulation of $P2Y_1$ or $P2Y_4$ receptor subtype markedly inhibited ACh-activated I_{GIRK} currents by G_q-PLC pathway signaling, although the two receptors were also weakly coupled to $G_{i/o}$ protein to transiently activate I_{GIRK}. On the contrary, $P2Y_2$ and $P2Y_{12}$ receptor subtypes were coupled with $G_{i/o}$ protein to persistently activate I_{GIRK}.

Materials and methods

Heterologous expression of cDNA in CHO cells

Full-length cDNA encoding rat GIRK1 subcloned into the pCI expression vector was a kind gift from Dr. LY Jan (Department of Physiology and Biochemistry, Howard Hughes Medical Institute, University of California). Full-length cDNA encoding rat GIRK4 subcloned into the pCDNA3 expression vector was kindly provided by Dr. JP Adelman (Department of Molecular and Medical Genetics, Oregon Health and Sciences University). Full-length cDNA encoding rat type I phosphatidylinositol-4-phosphate-5-kinase (PI4P-5K) subcloned into pCDNA3 expression vector was generously donated by Dr. Y Oka (Third Department of Internal Medicine, Yamaguchi University School of Medicine, Japan). Full-length cDNA encoding human M_2, α_1, $P2Y_1$, $P2Y_2$, $P2Y_4$, $P2Y_{12}$ receptors and regulator of G protein signaling 2 (RGS_2) subcloned individually into $pCDNA3.1^+$ were all obtained from the University of Missouri–Rolla cDNA Resource Center (Rolla, MO). The experimental cDNAs were transiently transfected into CHO cells together with green fluorescent protein (GFP) cDNA [0.5 μg GFP +1 μg GIRK1+1 μg GIRK4+1 μg P2Ys (or α_1)+1 μg M_2] by using Lipofectamine (Invitrogen Life Technologies, Inc. Carlsbad, CA, USA) according to the manufacturer's instructions. Two micrograms of PI4P-5K or RGS_2 cDNA was co-transfected in subset experiments. The transfected cells were cultured in DMEM/Ham's F-12 medium (Nakalai Tesque Inc., Kyoto, Japan) supplemented with 10% fetal bovine serum (GIBCO) and antibiotics (100 U/ml penicillin and 100 μg/ml streptomycin) in a humidified incubator with 5% CO_2 and 95% air at 37°C. The cultures were passaged every 4 to 5 days using a brief trypsin–EDTA treatment. The trypsin-EDTA treated cells were seeded onto glass coverslips in a petri dish for later patch-clamp experiments.

Solutions and chemicals

The pipette solution contained (mM) 70 potassium aspartate, 40 KCl, 10 KH_2PO_4, 1 $MgSO_4$, 3 Na_2-ATP (Sigma), 0.1 Li_2-GTP (Roche Diagnostics GmbH, Mannheim, Germany), 5 EGTA, and 5 Hepes, and pH was adjusted to 7.2 with KOH. The extracellular solution contained (mM) 140 NaCl, 5.4 KCl, 1.8 $CaCl_2$, 0.5 $MgCl_2$, 0.33 NaH_2PO_4, 5.5 glucose, and 5.0 Hepes, and pH was adjusted to 7.4 with NaOH. Agents added to the extracellular solutions included ACh (Sigma Chemical Co., St. Louis, MO, USA), ATP (Sigma), uridine triphosphate (UTP, Sigma), bisindolylmaleimide 1 (BIS-1, Sigma), chelerychrine (CHE, Sigma), and phenylephrine (PHE, Sigma). ACh, ATP, UTP, and PHE were dissolved in the distilled water to yield 10 mM or 30

mM stock solutions. BIS-1 and CHE were dissolved in dimethyl sulfoxide (DMSO, Sigma) to yield stock solutions of 200 μM and 5 mM, respectively. Phosphatidylinositol 4,5-bisphosphate (PIP_2; Calbiochem, San Diego, CA, USA) was directly dissolved in the control pipette solution at a concentration of 50 μM with 30 min sonication on ice. In a subset of experiments, the cells were pre-incubated with 5 μg/ml PTX (Seikagaku, Japan) for at least 2 h to inhibit a PTX-sensitive G protein, as previously described [16].

Electrophysiological recordings and data analysis

The cells attached to glass coverslips were transferred to a 0.5-ml recording chamber perfused with extracellular solution at 1–2 ml/min after 48 h of transfection. The chamber was mounted on the stage of an inverted microscope (ECLIPSE TE2000-U; Nikon, Tokyo, Japan) and maintained at 25°C. Patch-clamp experiments were conducted on GFP-positive cells. Whole-cell membrane currents were recorded with an EPC-8 patch-clamp amplifier (HEKA, Lambrecht, Germany), and data were low-pass filtered at 1 kHz, acquired at 5 kHz through an LIH-1600 analog-to-digital converter (HEKA) and stored on a hard disc drive, using the PulseFit software program (HEKA). Patch pipettes were fabricated from borosilicate glass capillaries (Narishige, Japan) using a horizontal microelectrode puller (P-97; Sutter Instrument Co., USA), and the tips were then fire-polished using a microforge. Patch pipettes had a resistance of 2.5–4.0 MΩ when filled with the pipette solution. Membrane currents were measured at a holding potential of −40 mV or during the voltage ramp protocol (dV/dt=±0.4 V/s), which consisted of an ascending (depolarizing) phase from the holding potential to +50 mV followed by a descending (hyperpolarizing) phase to −130 mV. The current–voltage (I–V) relationship was determined during descending phase.

All of the averaged data are expressed as the mean ± SEM, with the number of experiments shown in parentheses. Statistical comparisons were analyzed using either Student's unpaired t test or ANOVA followed by Dunnett's *post hoc*, as appropriate. Differences were considered to be statistically significant if a value of $P<0.05$ was obtained.

Results

The nature of I_{GIRK} during exposure to ATP in CHO cells expressing $P2Y_1$ receptor

The effect of extracellular ATP on I_{GIRK} was examined in cells transfected with $P2Y_1$ receptor by measuring whole-cell membrane currents at a holding potential of −40 mV and during hyperpolarizing voltage ramps from +50 to −130 mV. The bath application of 10 μM ATP initially evoked a rapid outward shift of the holding current (I_{GIRK} activation), which then progressively declined to the baseline level within ~1–2 min (a subsequent inward shift, Fig. 1a) despite the continued presence of the agonist.

Figure 1b illustrates the membrane currents during hyperpolarizing voltage ramps, recorded before and during application of ATP. The membrane current was calculated by digital subtraction of the current traces under control conditions from that shortly after ATP application and showed an inward rectification (Fig. 1c). $I_{K,ACh}$ is activated by a membrane-delimited pathway involving a PTX-sensitive G protein ($G_{i/o}$) in guinea-pig atrial myocytes [24]. The present experiment also found that pre-exposure to 5 μg/ml PTX for 2 h abolished the action of extracellular ATP (Fig. 1d), suggesting that a PTX-sensitive G protein mediates the activation of I_{GIRK} by $P2Y_1$ receptor stimulation.

The functional regulation of $P2Y_1$ receptor was further analyzed using 10 μM ACh to induce an activation of I_{GIRK} at −40 mV (Fig. 2a). The further addition of ATP initially had an additive effect on ACh-activated I_{GIRK} but then markedly inhibited the current (Fig. 2a; the number of cells

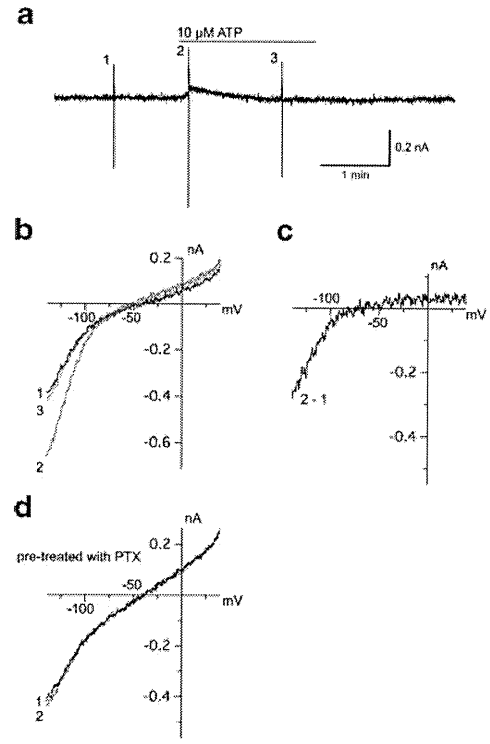

Fig. 1 Effect of ATP on the activation of I_{GIRK} in CHO cells transfected with $P2Y_1$ receptor. **a** The whole-cell currents recorded at a holding potential of −40 mV and during exposure to 10 μM ATP. **b** Superimposed I–V relationships measured during the voltage ramps applied at the points indicated by numbers (*1–3*) in panel (**a**). **c** I–V relationship obtained by digital subtraction of current traces as indicated. **d** After pretreatment with 5 μg/ml PTX for 2 h, the I–V relationships were measured during the voltage ramps

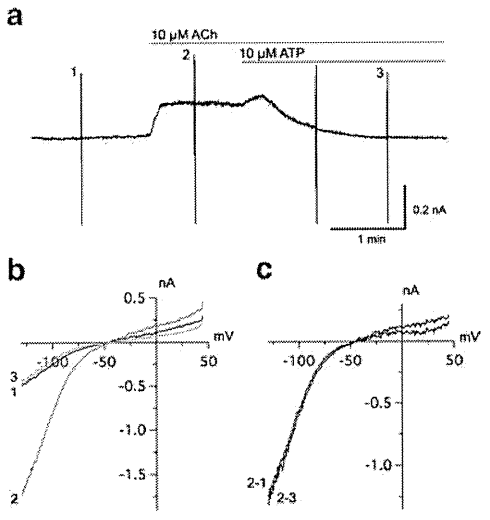

Fig. 2 Inhibition of ACh-activated I_{GIRK} by ATP. **a** The whole-cell currents recorded at a holding potential of −40 mV and during voltage ramps applied before (*1*), during exposure to 10 μM ACh (*2*), and after further addition of 10 μM ATP (*3*). **b** Superimposed *I–V* relationships measured during the voltage ramps applied at the points indicated by numerals (*1–3*) in panel (**a**). **c** Superimposed *I–V* relationships for the difference currents obtained by digital subtraction of current records as indicated. The voltage ramp traces were truncated for the purpose of presentation

positively responded to ATP was 18/19). The ACh-activated maximal I_{GIRK} was decreased by 92.44±10.61% (n=19), when measured 3 min after application of 10 μM ATP, which indicates that external ATP almost inhibited the ACh-activated I_{GIRK}. Figure 2b and c show that the ACh-activated I_{GIRK} current also exhibited an inwardly rectifying *I–V* relationship, which is consistent with the properties of $I_{K,ACh}$ in guinea-pig atrial myocytes. In addition, I_{GIRK} isolated by digital subtraction of the currents in the presence of ACh from that after ATP application also exhibited an inwardly rectifying *I–V* relationship.

In different sets of experiments, we examined the background currents and the expression ability of our CHO cell expression system. The results show that bath application of ACh and ATP could not induce any discernible currents in non-transfected cells (Fig. S1a) and in cells transfected only with GFP + GIRK1/GIRK4 (Fig. S1b). However, ACh evoked persistent I_{GIRK} currents in cells transfected with GFP + GIRK1/GIRK4 + M_2 (Fig. S1c), which was consistently inhibited by ATP when co-transfected with $P2Y_1$ in addition to GIRK subunits and M_2 (Fig. S1d). Figure S1e shows the representative image of the cells showing GFP expression. On the other hand, the inhibition of I_{GIRK} currents was not observed in cells without $P2Y_1$ transfection (Fig. S1c). These results indicate that functional expression of intrinsic P2Y and M_2 receptors was almost null in our CHO cell expression system, and all plasmids were successfully expressed in our cells. To exclude the possibility that the activation of I_{GIRK} was affected by G protein-coupled receptor–G protein interaction, we observed the effects of ATP on ACh-activated I_{GIRK} in CHO cells co-transfected lower doses (0.2–0.5 μg) of $P2Y_1$ together with 0.5 μg GFP +1 μg GIRK1/GIRK4+1 μg M_2. Figure S1f shows that the inhibition of ACh-activated I_{GIRK} by ATP in cells co-transfected with 0.2 μg $P2Y_1$ is almost the same as that co-transfected with 1 μg $P2Y_1$.

The modulation of RGS_2 on ATP-induced inhibition of I_{GIRK}

Regulators of G-protein signaling (RGS) proteins modulate the signal transduction via G protein-coupled receptors (GPCR). These proteins enhance GTP hydrolysis by accelerating the intrinsic GTPase activity of Gα-subunit, and thereby terminate the G protein activation cycle [4, 31, 39]. RGS_2 (one of the important inhibitor of $G_q\alpha$ subunit) was co-transfected with GIRK1/GIRK4, M_2 and $P2Y_1$ cDNAs to explore the inhibitory mechanism of ATP on I_{GIRK}. Figure 3a shows that the inhibitory action of ATP on ACh-activated I_{GIRK} was significantly attenuated with the co-expression of RGS_2. Figure 3c shows that the inhibitory degree of the ACh-activated I_{GIRK} was only 50.7± 9.1% (n=15) 3 min after exposure to 10 μM ATP, which

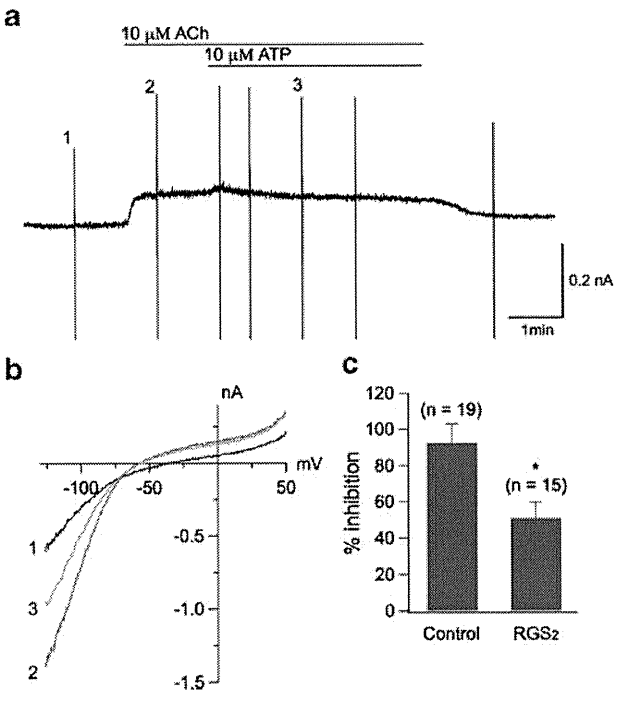

Fig. 3 The modulation of RGS_2 on the ATP-induced inhibition of I_{GIRK}. **a** Whole-cell currents recorded in CHO cell co-transfected with RGS_2 at a holding potential of −40 mV. **b** Superimposed *I–V* relationships measured during the voltage ramps applied at the points indicated by numerals (*1–3*) in panel (**a**). **c** ATP-induced inhibition of I_{GIRK} (*P<0.05 vs. control)

is significantly ($P<0.05$) lower than that of control (92.44± 10.61%, $n=19$). Therefore, the activation of G_q protein is involved in the ATP-induced inhibition of I_{GIRK}. Besides, our supplementary experiment data observed in CHO cells co-transfected 1 μg M_1 receptor (coupled with G_q) together with 0.5 μg GFP+1 μg GIRK1+1 μg GIRK4+1 μg M_2 (Fig. S3a) also supports the result that the activation of G_q protein is involved in the agonist-induced inhibition of I_{GIRK} in this experiment.

In order to further confirm the result that co-expression of RGS_2 led to the inhibition of the signal transduction via G_q protein-coupled receptors in our cell expression system, we co-transfected GFP + GIRK1/GIRK4+M_2+RGS_2 together with α_1-adrenergic receptor that has been generally accepted to be coupled to G_q [8]. Similar to the inhibition of ACh-activated I_{GIRK} currents by ATP, bath application of PHE (a selective α_1 receptor agonist, 30 μM) significantly inhibited the ACh-activated I_{GIRK} currents by 94.8±10.1% ($n=7$) in cells co-expressing α_1 receptor (Fig. S2a), whereas only by 40.3±5.4% ($n=5$, $P<0.01$) in cells co-expressing $RGS_2+\alpha_1$ receptor (Fig. S2b), implicating that the attenuation of I_{GIRK} inhibition by ATP in cells co-expressing RGS_2 is involved in blockade of G_q protein in our experiment.

Role of membrane PIP_2 in ATP-induced decline of I_{GIRK}

A previous study indicated that ATP receptor stimulation could inhibit the $I_{K,ACh}$ channels through depletion of membrane PIP_2 in guinea pig atrium [44]. PI4P-5K (the enzyme that catalyzes PIP_2 synthesis [11]) was co-expressed with GIRK1/GIRK4, M_2, and $P2Y_1$ cDNAs. Figure 4a shows that the co-expression of PI4P-5K markedly ($P<0.01$) prevented the inhibitory action of ATP on ACh-activated I_{GIRK}, compared with that in control (55.2±10.0%, $n=13$ vs. 92.44 ±10.61%, $n=19$; Fig. 4c). This result is consistent with the view that a characteristic progressive decline of I_{GIRK} in the presence of extracellular ATP is mediated through the depletion of membrane PIP_2.

If the reduction in membrane PIP_2 underlies the decline of I_{GIRK} during exposure to ATP, intracellular loading of exogenous PIP_2 may attenuate the inhibitory action of ATP on ACh-activated I_{GIRK}. As demonstrated in Fig. 5a and b, intracellular dialysis of 50 μM PIP_2 for 5–7 min through a recording pipette significantly reduced the inhibition degree of ACh-activated I_{GIRK} by ATP. The inhibition of I_{GIRK} (Fig. 5c) only reached 18.2±6.4% ($n=5$) 3 min after bath application of 10 μM ATP, which is markedly ($P<0.01$) lower than that of the control (92.44±10.61%, $n=19$). This result further indicates that the reduction in membrane PIP_2 is closely linked to the inhibitory action of ATP on I_{GIRK}.

PKC activation was previously reported to produce inhibitory action on $I_{K,ACh}$ [14, 22, 31, 35]. In our experiments, however, bath application of two different PKC

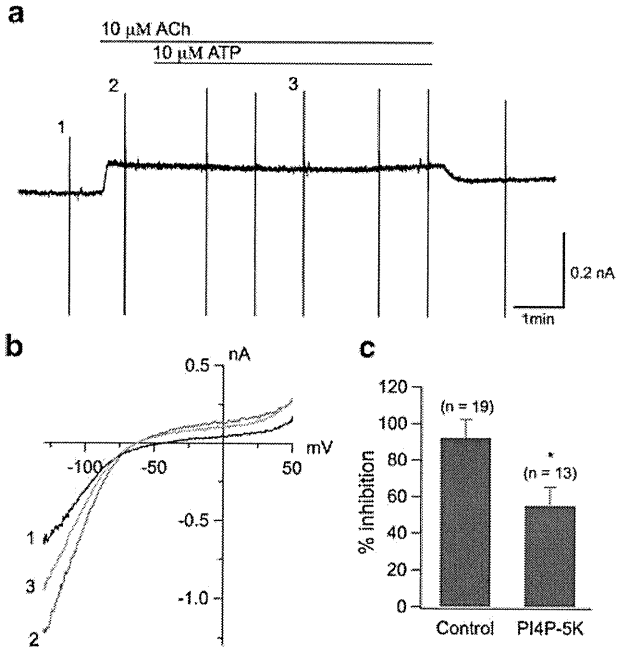

Fig. 4 Co-expression of PI4P-5K attenuated the ATP-induced inhibition of I_{GIRK}. **a** The whole-cell currents recorded in CHO cell co-transfected with PI4P-5K in the presence of ACh and ATP at a holding potential of −40 mV. **b** Superimposed *I–V* relationships measured during the voltage ramps applied at the points indicated by numerals (*1–3*) in panel (**a**). **c** ATP-induced inhibition of I_{GIRK} (*$P<0.05$ vs. control)

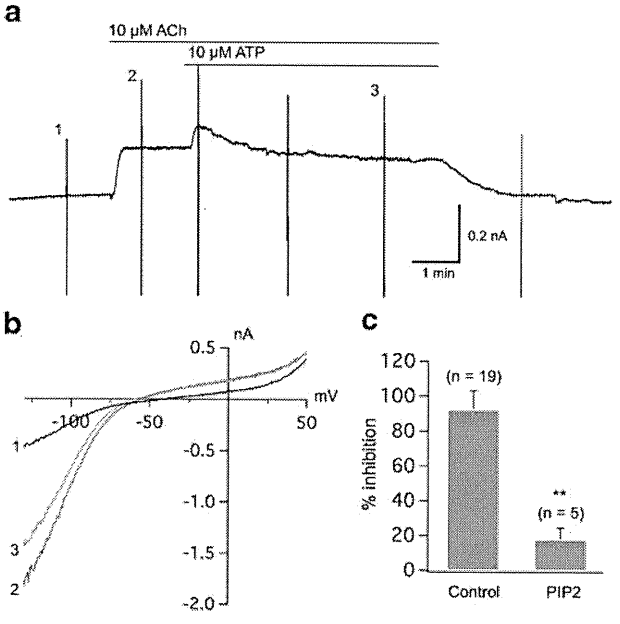

Fig. 5 Effect of PIP_2 (intracellularly loaded) on the ATP-induced inhibition of I_{GIRK}. **a** Whole-cell currents recorded with PIP_2 intracellular dialysis for 5–7 min at a holding potential of −40 mV, and then in the presence of ACh and ATP. **b** Superimposed *I–V* relationships measured during the voltage ramps applied at the points indicated by numerals (*1–3*) in panel (**a**). **c** ATP-induced inhibition of I_{GIRK} (**$P<0.01$ vs. control)

inhibitors, bisindolylmaleimide (BIS-1, 200 nM, Fig. 6a and b) and chelerythrine (CHE, 5 μM, Fig. 6b), did not significantly alter the inhibition degree of ACh-activated I_{GIRK} by ATP (control, 92.44±10.61%, n=19; BIS-I, 95.7±15.0%, n=7; CHE, 92.3±17.5%, n=6), thus suggesting that PKC activation is not involved in the ATP-induced inhibition of I_{GIRK} [7, 28].

Effects of P2Y receptor subtype stimulation on I_{GIRK}

Different P2Y receptor subtpes, namely $P2Y_2$, $P2Y_4$, and $P2Y_{12}$, were respectively transfected together with GIRK1/GIRK4 channels to explore the effects of the P2Y receptor stimulation on I_{GIRK}. In the experiment, 10 μM UTP was used as an alternative to ATP to activate $P2Y_2$ and $P2Y_4$ receptors because it seems that these two receptors are more sensitive to UTP [38, 41]. Figure 7a shows the representative I_{GIRK} traces elicited by stimulating $P2Y_2$, $P2Y_4$, and $P2Y_{12}$ receptors, respectively. The persistent I_{GIRK} currents elicited by the stimulation of $P2Y_2$ or $P2Y_{12}$ receptor suggest that little membrane PIP_2 was depleted, whereas the current evoked by the stimulation of $P2Y_4$ receptor was transient, which suggests that depletion of membrane PIP_2 occurred. Figure 7b and c shows the amplitudes of I_{GIRK} normalized to the peak amplitude one minute (I_{1min}/I_{peak}) and 3 min (I_{3min}/I_{peak}) after application of an agonist. The normalized amplitude of I_{GIRK} for $P2Y_2$ or $P2Y_{12}$ was significantly (P<0.01) larger than that of $P2Y_1$ both 1 and 3 min after application of an agonist, whereas the amplitude of I_{GIRK} for $P2Y_1$ or $P2Y_4$ 3 min after receptor stimulation was significantly (P<0.05) lower than that for the same receptor 1 min after receptor stimulation.

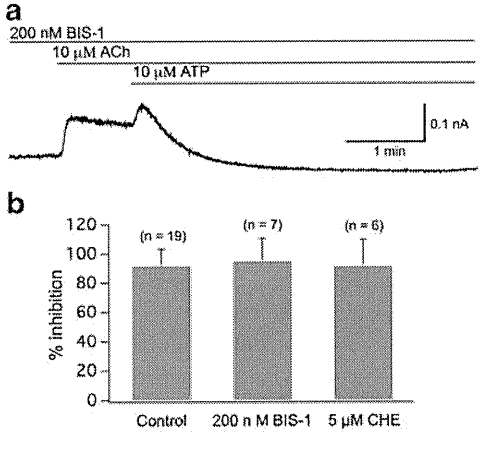

Fig. 6 PKC inhibitors did not attenuate the ATP-induced inhibition of I_{GIRK}. **a** The whole-cell currents recorded in CHO cell pre-treated with 200 nM BIS-1 in the presence of ACh and ATP at a holding potential of −40 mV. **b** ATP-induced inhibition of I_{GIRK} in the presence of 200 nM BIS-1 or 5 μM CHE

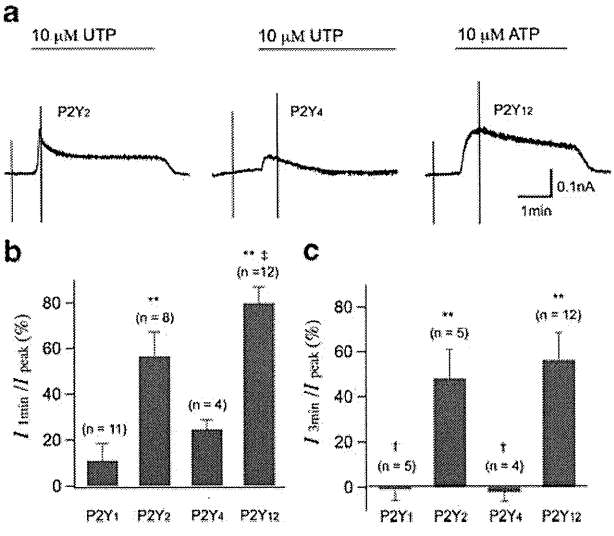

Fig. 7 Comparison of I_{GIRK} currents evoked by stimulating different P2Y receptor subtypes. **a** The whole-cell currents in CHO cells transfected with $P2Y_2$, $P2Y_4$, and $P2Y_{12}$ receptor subtypes at a holding potential of −40 mV. **b** Inhibition of I_{GIRK} 1 min after stimulation of $P2Y_2$, $P2Y_4$, and $P2Y_{12}$ receptors. **c** Inhibition of I_{GIRK} 3 min after stimulation of $P2Y_2$, $P2Y_4$, and $P2Y_{12}$ receptors (**P<0.01 vs. $P2Y_1$ or $P2Y_4$; $^{‡}P$<0.05 vs. $P2Y_2$; $^{†}P$<0.05 vs. I_{1min}/I_{peak})

Treatment with 10 μM ACh was first used to induce an I_{GIRK} current at −40 mV, and then 10 μM UTP or ATP was employed to stimulate $P2Y_2$, $P2Y_4$, or $P2Y_{12}$ to further examine the effects of $P2Y_s$ receptor stimulation on ACh-activated I_{GIRK}. Figure 8a and b shows that the nature of the current evoked by stimulating $P2Y_4$ receptor with UTP was almost the same as that elicited by stimulating $P2Y_1$ (Fig. 2). The inhibitory degree of ACh-activated I_{GIRK} by the stimulation of $P2Y_4$ was 99.6±22.5% (n=5), which was similar to that evoked by the stimulation of $P2Y_1$ receptor (Fig. 8c). Figure S3b and c shows that addition of an agonist (ATP or UTP) caused the ACh-activated I_{GIRK} to increase further (there was 1/13 cell co-transfected with $P2Y_2$ that did not respond to UTP). The addition activation of I_{GIRK} by the stimulation of $P2Y_2$ declined slightly, but still much higher than the ACh-activated I_{GIRK} level 3 min after treatment with UTP (Fig. S3b). On the other hand, the addition activation of I_{GIRK} by the stimulation of $P2Y_{12}$ almost did not decline (Fig. S3c).

Discussion

The activation of $I_{K,ACh}$ is due to the activation of $G_{i/o}$ protein [34]. The rapid activation phase of $I_{K,ACh}$ evoked by exposure to ATP is caused by stimulation of P2Y receptor, leading to a membrane-delimited, $G_{i/o}$-mediated channel activation in guinea-pig atrial myocytes [14, 25, 44]. However, there is no consensus on the mechanism of $I_{K,ACh}$

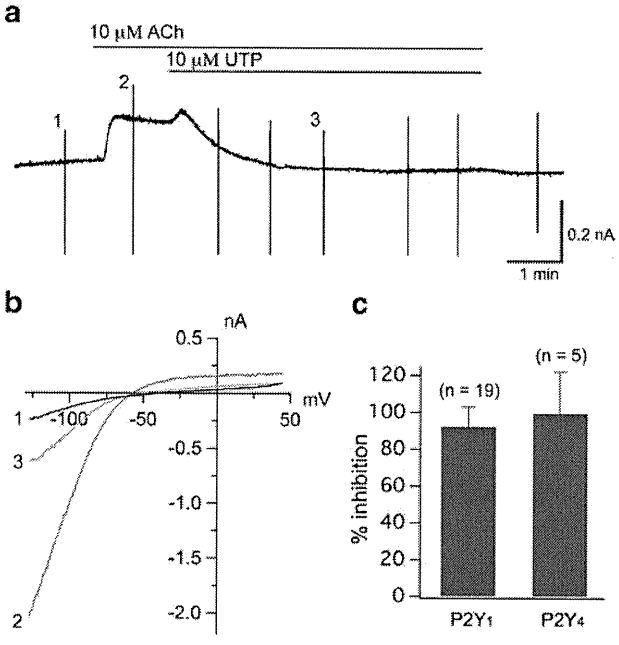

Fig. 8 Effect of $P2Y_4$ stimulation on ACh-activated I_{GIRK}. **a** The whole-cell currents recorded at a holding potential of −40 mV, and in the presence of ACh and UTP. **b** Superimposed *I–V* relationships measured during the voltage ramps applied at the points indicated by numerals (*1–3*) in panel (**a**). **c** Inhibitory degree of I_{GIRK} by the stimulation of $P2Y_1$ and $P2Y_4$ receptors

inhibition produced by agonists. Several groups [7, 14, 18, 25, 29, 44] reported that activation of PLC contributes to the inhibition of $I_{K,ACh}$ by decreasing membrane PIP_2. However, others [15, 23, 32, 36] suggest that the downstream activation of PKC underlies the inhibition of $I_{K,ACh}$. There are also some pieces of evidence to suggest that reduction in membrane PIP_2 and PKC activation are both involved in the $I_{K,ACh}$ inhibition by agonists such as carbachol [22] and ACh [17].

A previous study in the guinea-pig atrium indicated that the inhibition of $I_{K,ACh}$ by extracellular ATP is attenuated by blocking PLC activity with compound 48/80 and by exogenously adding PIP_2 in the atrial myocytes [44]. This observation suggests that the ATP-induced activation of PLC and the concomitant reduction of PIP_2 contribute to the inhibition of $I_{K,ACh}$ by ATP. In addition, RGS_2 protein is one of the important inhibitor of the $G_q\alpha$ subunit and terminates G_q signaling through its GTPase-activating protein mechanism [4, 31, 39]. The present experiment found that co-expression of RGS_2 significantly reduced the ATP-induced inhibition of I_{GIRK}, thus confirming the view that the inhibition of I_{GIRK} by ATP is mediated through the G_q protein-coupled P2Y receptors in native cardiac myocytes [14, 25]. The present study also demonstrated that the ATP-induced inhibition of I_{GIRK} is markedly attenuated by both co-expression of PI4P-5K and intracellular dialysis with PIP_2 in CHO cells. These data are consistent with a previous study in guinea-pig atrial myocytes [44] and support the view that a decrease in membrane PIP_2 is closely linked to the ATP-induced inhibition of $I_{K,ACh}$. In contrast to the study of Keselman et al. [17], however, the PKC inhibitor BIS-1 and CHE did not alter the inhibition of ATP on ACh-activated I_{GIRK}, thus indicating PKC activation might not be involved in the inhibition of I_{GIRK} by ATP [9, 28]. Taken together, the current data fully support the hypothesis that the reduction in membrane PIP_2 via activation of G_q-PLC is mainly responsible for the inhibition of $I_{K,ACh}$ channels by externally applying ATP.

Previous reports have indicated that $P2Y_1$, $P2Y_2$, and $P2Y_4$ receptor subtypes are coupled to PTX-insensitive G_q proteins that activate PLC and then produce a fall in membrane PIP_2 levels, whereas $P2Y_{12}$ receptor is only coupled to PTX-sensitive $G_{i/o}$ protein to inhibition of adenylate cyclase [1, 9, 37, 41]. However, the coupling to signaling transduction pathways appears to be much more complex. An example is that the G_q-coupled $P2Y_1$ receptor, known to inhibit GIRK channels, efficiently activates GIRK1/GIRK2 channels in cultured rat sympathetic neurons [12]. A sequence analysis also indicates that the two regions (the third intracellular loop and the C-terminal tail), implicated in G protein specificity, vary greatly among the P2Y receptor subtypes [40]. The present study found that the stimulation of $P2Y_1$ or $P2Y_4$ receptor evoked a transient activation of I_{GIRK} followed by a persistent inhibition (Figs. 1a and 7a), thus suggesting that a large amount of membrane PIP_2 was consumed via activation of G_q-PLC pathway. This result might implicate that the two receptors are mainly coupled to G_q protein. Contrary to previous reports [1, 9, 37, 41], however, the activation phase of I_{GIRK} evoked by the stimulation of these two receptors reflects the existence of $G_{i/o}$ coupling although it might be relatively weak. In contrast, the stimulation of $P2Y_2$ or $P2Y_{12}$ receptor induced a persistent activation of I_{GIRK} (Fig. 7a), indicating that little membrane PIP_2 was consumed and resultantly implicating that these two receptors are mainly coupled to $G_{i/o}$ protein. Bodor and colleagues have found that purified $P2Y_{12}$ receptor can form a functional receptor when reconstituted with G_i protein, but not when reconstituted with G_q protein [6]. This is consistent with the present finding that the $P2Y_{12}$ receptor is coupled to $G_{i/o}$ protein to activate I_{GIRK}. In addition, the decay I_{GIRK} evoked by the stimulation of $P2Y_2$ was relatively rapid in comparison to the $P2Y_{12}$, suggesting that some amount of membrane PIP_2 was still consumed during the stimulation of $P2Y_2$ and resultantly implicating that $P2Y_2$ is also weakly coupled to G_q protein. The $P2Y_2$ receptor is generally classified to the (PTX-resistant) G_q-coupled subfamily [9, 19, 41]. However, the data in the present study suggested that $P2Y_2$ is also coupled to $G_{i/o}$ protein as suggested by other researchers [37], though they

believed that $P2Y_2$ receptor primarily mediates its function through coupling to G_q. Furthermore, these data are also supported by the fact that $P2Y_2$ receptor is sensitive to PTX in stable expressed astrocytoma cells [33] and in human erythroleukemia cells [2].

There is an abundant expression of $P2Y_2$ mRNA in both human atria and ventricles, whereas the mRNA level of $P2Y_2$ is lower than that of $P2Y_1$ or $P2Y_4$ in mouse cardiomyocytes [43]. Musa and colleagues [30] have also indicated that the $P2Y_2$ mRNA level is the most abundant of the eight P2Y receptors in the human right atrium, but is lower than $P2Y_1$ in human sinoatrial node (SAN). They also found that the distribution of P2Y receptor subtypes in rat right atrium, left ventricle, and SAN is quite different with those in the human heart. These results indicate that the P2Y receptor expression varies greatly in the heart, implicating that responses to the stimulation of P2Y receptor are also diverse in different types of cardiac cells. The current study may contribute to understanding the precise regulatory mechanisms underlying the cardiac signaling pathway mediated by P2Y receptors.

Acknowledgements This study was supported by grants (No. 22590205 and No. 22590206) from the Ministry of Education, Science, and Culture of Japan; the Uehara Memorial Foundation; and health science research grants from the Ministry of Health, Labor and Welfare of Japan for Clinical Research on Measures for Intractable Diseases.

Ethical standards The authors declare that the experiment comply with the current laws of Japan.

Conflict of interest The authors declare that they have no conflict of interest.

References

1. Abbracchio MP, Burnstock G, Boeynaems JM, Barnard EA, Boyer JL, Kennedy C, Knight GE, Fumagalli M, Gachet C, Jacobson KA, Weisman GA (2006) International Union of Pharmacology LVIII: update on the P2Y G protein-coupled nucleotide receptors: from molecular mechanisms and pathophysiology to therapy. Pharmacol Rev 58:281–341
2. Baltensperger K, Porzig H (1997) The P_{2U} purinoceptor obligatorily engages the heterotrimeric G protein G_{16} to mobilize intracellular Ca^{2+} in human erythroleukemia cells. J Biol Chem 272:10151–10159
3. Banfi C, Ferrario S, De Vincenti O, Ceruti S, Fumagalli M, Mazzola A, D'Ambrosi N, Volonte C, Fratto P, Vitali E, Burnstock G, Beltrami E, Parolari A, Polvani G, Biglioli P, Tremoi E, Abbracchio MP (2005) P2 receptors in human heart: upregulation of P2X6 in patients undergoing heart transplantation, interaction with TNFalpha and potential role in myocardial cell death. J Mol Cell Cardiol 39:929–939
4. Bernstein LS, Ramineni S, Hague C, Cladman W, Chidiac P, Levey AL, Hepler JR (2004) RGS2 binds directly and selectively to the M1 muscarinic acetylcholine receptor third intracellular loop to modulate Gq/11alpha signaling. J Biol Chem 279:21248–21256
5. Birnbaumer L (2007) Expansion of signal transduction by G proteins. The second 15 years or so: from 3 to 16 α subunits plus $\beta\gamma$ *dimmers. Biochim Biophys Acta 1768:772–793*
6. Bodor ET, Waldo GL, Hooks SB, Corbitt J, Boyer JL, Harden TK (2003) Purification and functional reconstitution of the human $P2Y_{12}$ receptor. Mol Pharmacol 64:1210–1216
7. Cho H, Lee D, Lee SH, Ho WK (2005) Receptor-induced depletion of phosphatidylinositol 4,5-bisphosphate inhibits inwardly rectifying K^+ channels in a receptor-specific manner. Proc Natl Acad Sci USA 102:4643–4648
8. Docherty JR (2010) Subtypes of functional alpha1-adrenoceptor. Cell Mol Life Sci 67:405–417
9. Erb L, Liao Z, Seye CI, Weisman GA (2006) P2 receptors: intracellular signaling. Pflugers Arch 452:552–562
10. Erlinge D, Burnstock G (2008) P2 receptors in cardiovascular regulation and disease. Purinergic Signalling 4:1–20
11. Falkenburger BH, Jensen JB, Hille B (2010) Kinetics of PIP2 metabolism and KCNQ2/3 channel regulation studied with a voltage-sensitive phosphatase in living cells. J Gen Physiol 135:99–114
12. Filippov AK, Fernandez-Fernandex JM, Marsh SJ, Simon J, Barnard EA, Brown DA (2004) Activation and inhibition of neuronal G protein-gated inwardly rectifying K(+) channels by P2Y nucleotide receptors. Mol Pharmacol 66:468–477
13. Friel DD, Bean BP (1990) Dual control by ATP and acetylcholine of inwardly rectifying K^+ channels in bovine atrial cells. Pflugers Arch 415:651–657
14. Hara Y, Nakaya H (1997) Dual effects of extracellular ATP on the muscarinic acetylcholine receptor-operated K^+ current in guinea-pig atrial cells. Eur J Pharmacol 324:295–303
15. Hill JJ, Peralta EG (2001) Inhibition of a G_i-activated potassium channel (GIRK1/4) by the G_q-coupled m1 muscarinic acetylcholine receptor. J Biol Chem 276:5505–5510
16. Hwang TC, Horie M, Nairn AC, Gadsby DC (1992) Role of GTP-binding proteins in the regulation of mammalian cardiac chloride conductance. J Gen Physiol 99:465–489
17. Keselman I, Fribourg M, Felsenfeld DP, Logothetis DE (2007) Mechanism of PLC-mediated Kir3 current inhibition. Channels (Austin) 1:113–123
18. Kobrinsky E, Mirshahi T, Zhang H, Jin T, Logothetis DE (2000) Receptor-mediated hydrolysis of plasma membrane messenger PIP2 leads to K^+-current desensitization. Nat Cell Biol 2:507–514
19. Koles L, Gerevich Z, Oliveira JF, Zadori ZS, Wirkner K, Illes P (2008) Interaction of P2 purinergic receptors with cellular macromolecules. Naunyn-Schmiedeberg's Arch Pharmacol 377:1–33
20. Krapivinsky G, Gordon EA, Wickman K, Velimirovic B, Krapivinsky L, Clapham DE (1995) The G-protein-gated atrial K^+ channel I_{KACh} is a heteromultimer of two inwardly rectifying K^+-channel proteins. Nature 374:135–141
21. Kurachi Y, Nakajima T, Sugimoto T (1986) On the mechanism of activation of muscarinic K^+ channels by adenosine in isolated atrial cells: involvement of GTP-binding proteins. Pflugers Arch 407:264–274
22. Leaney JL, Dekker LV, Tinker A (2001) Regulation of a G protein-gated inwardly rectifying K^+ channel by a Ca^{2+}-independent protein kinase C. J Physiol 534:367–379
23. Mao J, Wang X, Chen F, Wang R, Rojas A, Shi Y, Piao H, Jiang C (2004) Molecular basis for the inhibition of G protein-coupled inward rectifier K^+ channels by protein kinase C. Proc Natl Acad Sci USA 101:1087–1092
24. Matsuura H, Sakaguchi M, Tsuruhara Y, Ehara T (1996) Activation of the muscarinic K^+ channel by P_2-purinoceptors via pertussis toxin-sensitive G proteins in guinea-pig atrial cells. J Physiol 490:659–671

25. Matsuura H, Ehara T (1996) Modulation of the muscarinic K^+ channel by P_2-purinoceptors in guinea-pig atrial myocytes. J Physiol 497:379–393
26. Matsuura H, Ehara T (1992) Activation of chloride current by purinergic stimulation in guinea pig heart cells. Circ Res 70:851–855
27. Matsuura H, Ehara T (1997) Selective enhancement of the slow component of delayed rectified K^+ current in guinea-pig atrial cells by external ATP. J Physiol 503:45–54
28. Matsuura H, Tsuruara Y, Sakaguchi M, Ehara T (1996) Enhancement of delayed rectifier K^+ current by P_2-purinoceptor stimulation in guinea-pig atrial. J Physiol 490:647–658
29. Meyer T, Wellner-Kienitz MC, Biewald A, Bender K, Eickel A, PottlT L (2001) Depletion of phosphatidylinositol 4,5-bisphosphate by activation of phospholipase C-coupled receptors causes slow inhibition but not desensitization of G protein-gated inward rectifier K^+ current in atrial myocytes. J Biol Chem 276:5650–5658
30. Musa H, Tellez JO, Chandler NJ, Greener ID, Maczewski M, Mackiewicz U, Beresewicz A, Molenaar P, Boyett MR, Dobrzynski H (2009) P2 purinergic receptor mRNA in rat and human sinoatrial node and other heart regions. Naunyn Schmiedebergs Arch Pharmacol 379:541–549
31. Neitzel KL, Hepler JR (2006) Cellular mechanisms that determine selective RGS protein regulation of G protein-coupled receptor signaling. Semin Cell Dev Biol 17:383–389
32. Nikolov EN, Ivanova-Nikolova TT (2004) Coordination of membrane excitability through a GIRK1 signaling complex in the atria. J Biol Chem 279:23630–23636
33. Parr CE, Sullivan DM, Paradiso AM, Lazarowski ER, Burch LH, Olsen JC, Erb L, Weisman GA, Boucher RC, Turner JT (1994) Cloning and expression of a human P_{2U} nucleotide receptor, a target for cystic fibrosis pharmacotherapy. Proc Natl Acad Sci USA 91:3275–3279
34. Pfaffinger PJ, Martin JM, Hunter DD, Nathanson NM, Hille B (1985) GTP-binding proteins couple cardiac muscarinic receptors to a K channel. Nature 317:536–538
35. Soejima M, Noma A (1984) Mode of regulation of the ACh-sensitive K-channel by the muscarinic receptor in rabbit atrial cells. Pflugers Arch 400:424–431
36. Stevens EB, Shah BS, Pinnock RD, Lee K (1999) Bombesin receptors inhibit G protein-coupled inwardly rectifying K^+ channels expressed in *Xenopus* oocytes through a protein kinase C-dependent pathway. Mol Pharmacol 55:1020–1027
37. Talasila A, Germack R, Dickenson JM (2009) Characterization of P2Y receptor subtypes functionally expressed on neonatal rat cardiac myofibroblasts. Br J Pharmacol 58:339–353
38. Thaning P, Bune LT, Hellsten Y, Pilegaard H, Saltin B, Rosenmeier JB (2010) Attenuated purinergic receptor function in patients with type 2 diabetes. Diabetes 59:182–189
39. Tsang S, Woo AY, Zhu W, Xiao RP (2010) Deregulation of RGS2 in cardiovascular diseases. Front Biosci (Schol Ed) 2:547–557
40. Vassort G (2001) Adenosine 5′-triphosphate: a P2-purinergic agonist in the myocardium. Physiol Rev 81:767–806
41. Von Kugelgen I (2006) Pharmacological profiles of cloned mammalian P2Y-receptor subtypes. Pharmacol Ther 110:415–432
42. Waldo GL, Harden TK (2004) Agonist binding and Gq-stimulating activities of the purified human $P2Y_1$ receptor. Mol Pharmacol 65:426–436
43. Wihlborg AK, Balogh J, Wang L, Borna C, Dou Y, Joshi BV, Lazarowski E, Jacobson KA, Arner A, Erlinge D (2006) Positive inotropic effects by uridine triphosphate (UTP) and uridine diphosphate (UDP) via $P2Y_2$ and $P2Y_6$ receptors on cardiomyocytes and release of UTP in man during myocardial infarction. Circ Res 98:970–976
44. Yasuda Y, Matsuura H, Ito M, Matsumoto T, Ding WG, Horie M (2005) Regulation of the muscarinic K^+ channel by extracellular ATP through membrane phosphatidylinositol 4,5-bisphosphate in guinea-pig atrial myocytes. Br J Pharmacol 145:156–165

Regional cooling facilitates termination of spiral-wave reentry through unpinning of rotors in rabbit hearts

Masatoshi Yamazaki, MD, PhD,*† Haruo Honjo, MD, PhD,* Takashi Ashihara, MD, PhD,‡ Masahide Harada, MD, PhD,* Ichiro Sakuma, PhD,§ Kazuo Nakazawa, PhD,‖ Natalia Trayanova, PhD, FHRS, FAHA,¶ Minoru Horie, MD, PhD,‡ Jérôme Kalifa, MD, PhD,† José Jalife, MD, FHRS,† Kaichiro Kamiya, MD, PhD,* Itsuo Kodama, MD, PhD*

*From the *Department of Cardiovascular Research, Research Institute of Environmental Medicine, Nagoya University, Nagoya, Japan, †Center for Arrhythmia Research, University of Michigan, Ann Arbor, Michigan, ‡Department of Cardiovascular and Respiratory Medicine, Shiga University of Medical Science, Otsu, Japan, §Graduate School of Engineering, The University of Tokyo, Tokyo, Japan, ‖National Cardiovascular Center, Research Institute, Suita, Japan, ¶Institute for Computational Medicine, Johns Hopkins University, Baltimore, Maryland.*

BACKGROUND Moderate global cooling of myocardial tissue was shown to destabilize 2-dimensional (2-D) reentry and facilitate its termination.

OBJECTIVE This study sought to test the hypothesis that regional cooling destabilizes rotors and facilitates termination of spontaneous and DC shock-induced subepicardial reentry in isolated, endocardially ablated rabbit hearts.

METHODS Fluorescent action potential signals were recorded from 2-D subepicardial ventricular myocardium of Langendorff-perfused rabbit hearts. Regional cooling (by 5.9°C ± 1.3°C) was applied to the left ventricular anterior wall using a transparent cooling device (10 mm in diameter).

RESULTS Regional cooling during constant stimulation (2.5 Hz) prolonged the action potential duration (by 36% ± 9%) and slightly reduced conduction velocity (by 4% ± 4%) in the cooled region. Ventricular tachycardias (VTs) induced during regional cooling terminated earlier than those without cooling (control): VTs lasting >30 seconds were reduced from 17 of 39 to 1 of 61. When regional cooling was applied during sustained VTs (>120 seconds), 16 of 33 (48%) sustained VTs self-terminated in 12.5 ± 5.1 seconds. VT termination was the result of rotor destabilization, which was characterized by unpinning, drift toward the periphery of the cooled region, and subsequent collision with boundaries. The DC shock intensity required for cardioversion of the sustained VTs decreased significantly by regional cooling (22.8 ± 4.1 V, n = 16, vs 40.5 ± 17.6 V, n = 21). The major mode of reentry termination by DC shocks was phase resetting in the absence of cooling, whereas it was unpinning in the presence of cooling.

CONCLUSION Regional cooling facilitates termination of 2-D reentry through unpinning of rotors.

KEYWORDS Spiral-wave reentry; Regional myocardial cooling; Unpinning; Optical mapping; Ventricular tachyarrhythmia

ABBREVIATIONS **2-D** = two-dimension; **3-D** = three-dimension; **APD** = action potential duration; **BCL** = basic cycle length; **BDM** = 2,3-butandione monoxime; **CV** = conduction velocity; **FBL** = functional block line; **ICD** = implantable cardioverter-defibrillator; **LV** = left ventricle; **PS** = phase singularity; **RC** = regional cooling; **SW** = spiral wave; **VF** = ventricular fibrillation; **VT** = ventricular tachycardia

(Heart Rhythm 2012;9:107–114)

Introduction

High-energy DC shock application by implantable cardioverter-defibrillator (ICD) is the most effective procedure for preventing sudden cardiac death resulting from ventricular tachycardia/ventricular fibrillation (VT/VF). Large-scale clinical trials have demonstrated that ICD therapy is superior over any pharmacological therapy to prevent cardiac death.[1,2] The usefulness of ICD therapy currently available is, however, limited by a number of adverse effects of high-energy shocks, such as myocardial damages causing arrhythmias, increased pacing threshold,[3,4] and mechanical dysfunction giving rise to hemodynamic deterioration.[5] In addition, painful DC shocks by ICD often cause serious psychological disorders.[6,7] Theoretical and experimental studies have revealed that spiral-wave (SW) reentry rotating around a functional obstacle is the major mechanism of VT/VF.[8,9] Arguably, should SW reentry be regulatable by procedures other than DC shocks or those combined with low-energy shocks, it could lead to innovative therapeutic

This study was supported by Grant-in-Aid for Scientific Research (B) 19390210 and (C) 20590860 from the Japanese Society for Promotion of Sciences and Grant-in-Aid for Scientific Research on Innovative Area 22136010 from the Ministry of Education, Culture, Sports, Science and Technology, Japan. **Address reprint requests and correspondence:** Dr. Haruo Honjo, Department of Cardiovascular Research, Research Institute of Environmental Medicine, Nagoya University, Furo-cho, Chikusa-ku, Nagoya 464-8601, Japan. E-mail address: honjo@riem.nagoya-u.ac.jp.

1547-5271/$ -see front matter doi:10.1016/j.hrthm.2011.08.013

modalities for prevention of arrhythmic death. Although several conceptual approaches have been proposed to terminate SW reentry by low-energy DC application, e.g., resonant drift,[10,11] controlling chaos,[12] synchronized pacing,[13,14] and unpinning of SWs,[15,16] feasibility of these approaches has not yet been validated. In isolated rabbit hearts, we have previously shown that moderate hypothermia facilitates termination of VT through destabilization (unpinning) of SW reentry.[17] Using high-density electrode mapping in rabbit hearts, Boersma et al[18] demonstrated that regional cooling (RC) of the ventricle during programmed electrical stimulation prevented stabilization of functional reentry and resulted in only brief episodes of polymorphic VT that terminated spontaneously. Here we hypothesized that moderate RC of the ventricular myocardium could be a novel procedure to destabilize already-established and sustained VT and lead to its termination. To test this hypothesis, we carried out high-resolution optical mapping experiments in 2-dimensional (2-D) ventricular myocardium.

Methods

Experimental model and optical mapping

The protocol was approved by the Institutional Animal Care and Use Committee at Nagoya University. The experimental model and procedures of optical mapping are essentially the same as reported previously.[17,19,20] Briefly, optical membrane potential signals were recorded from a 2-D ventricular muscle layer of Langendorff-perfused rabbit hearts subjected to endocardial cryoablation; 2,3-butandione monoxime (BDM) was applied to minimize motion artifacts. Action potential duration (APD) and conduction velocity (CV) were measured during constant pacing (basic cycle length [BCL] 180 to 400 ms) from the apex. The details of experimental procedures and data analysis are described in the Online Supplemental Methods.

RC

The temperature of the central region of the left ventricular (LV) free wall was temporarily reduced by applying a transparent cooling device (diameter, 10 mm) perfused with cold water and in abutting contact with the epicardial surface (Figure 1A). In pilot experiments using thermography (TVS-200, Nippon Avionics, Tokyo, Japan) (Figure 1B), we confirmed that the temperature in the target area was decreased by 5.9°C ± 1.3°C (n = 7, $P < .05$) from baseline (36.0°C). The temperature change was reversed completely after removal of the device. Temperature outside the cooled region remained unchanged.

Experimental protocols

Reentrant VTs (lasting ≥3 beats) were induced by modified cross-field stimulation using 1 of 2 protocols. First, in 8 hearts, VTs were induced before and 20 seconds after application of RC to compare their duration and dynamics. Second, in 15 additional hearts, sustained VTs (>120 seconds) were induced and RC was applied to observe its effects on VT duration and dynamics. If the sustained VTs did not terminate during the 30-second observation period of RC, 10-ms monophasic DC shocks were applied at in-

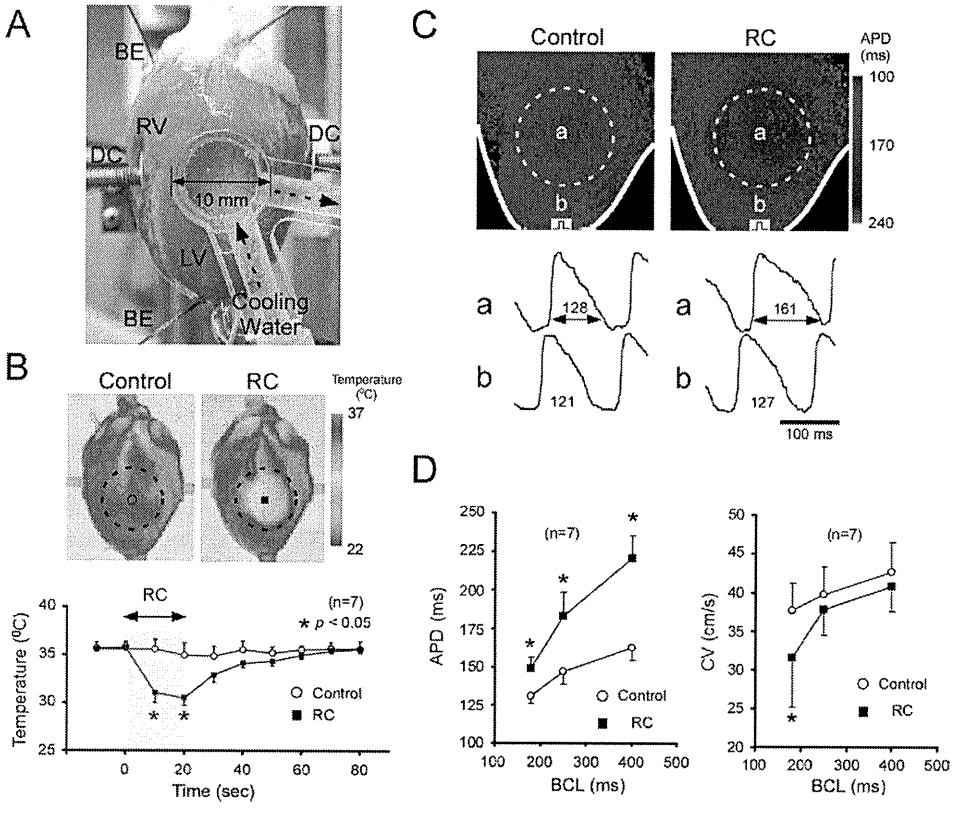

Figure 1 RC of 2-D rabbit hearts. **A:** A transparent cooling device (diameter, 10 mm) was in contact with the LV subepicardial surface, and water (20°C) was circulated inside the device. **B:** Thermography images (top) and changes of temperature (bottom) in response to RC. Those without RC served as control. *$P < .05$ vs control. **C:** Changes of APD (BCL, 400 ms) in response to RC. Top, APD color gradient maps with and without RC (control); bottom, optical action potential signals inside (a) and outside (b) the RC region. Numerals are APD (in ms). **D:** Effects of RC on APD (left) and CV (right) in the RC region at BCLs 180 to 400 ms. *$P < .05$ vs control (without RC). 2-D = two-dimension; APD = action potential duration; BCL = basic cycle length; BE = electrodes for recording distant bipolar electrograms; CV = conduction velocity; DC = paddle electrodes for DC-application; LV = left ventricle; RC = regional cooling.

creasing or decreasing voltage (by 5 to 10 V in steps from 25 V) to determine the threshold intensity for cardioversion. Sustained VTs without RC served as control subjects.

In 6 rabbits, effects of RC on VT/VF were examined in 3-dimensional (3-D) ventricles without cryoablation. Sustained VT/VFs (>120 seconds) were induced, and cardioversion by RC alone or in combination with DC shocks (8/2-ms biphasic, 25 to 100 V) was attempted.

Statistical analysis

Data are expressed as mean ± SD. Statistical comparisons were performed by 2-way analysis of variance with Bonferroni post hoc test or Welch 2-sample t test when appropriate. Differences were considered significant when $P < .05$.

Results

APD and CV during constant pacing

Effects of RC on APD and CV were examined in 7 hearts. Representative changes in APD (BCL, 400 ms) are shown in Figure 1C. Cooling (20 seconds) increased APD in the RC region, whereas APD outside the RC region was unchanged. Figure 1D summarizes the changes of APD and CV in the RC region. RC caused a significant increase of APD (BCLs, 180 to 400 ms); the longer the BCL, the greater the APD prolongation. RC decreased CV, although the changes remained statistically insignificant at BCLs 250 and 400 ms.

In 3 hearts, all of the RC-induced changes of APD and CV were reversed completely within 60 seconds after removal of the cooling device (data not shown).

VT induced during RC application

In 8 hearts, VTs were induced before (control) and 20 seconds after RC. In control subjects, 18 of 39 VTs (46%) terminated within 5 seconds, 4 VTs (10%) terminated in 5 to 30 seconds, and 17 VTs (44%) persisted for >30 seconds. During RC, in contrast, 58 of 61 VTs (95%) terminated within 5 seconds, 2 TVs (3%) terminated in 5 to 30 seconds, and 1 VT (2%) persisted >30 seconds. Thus, most of VTs induced during RC terminated earlier than in control subjects. The VT cycle length during RC (178 ± 20 ms, n = 61) was significantly longer compared with control subjects (143 ± 23 ms, n = 39, $P < .05$). Reversibility of the RC effects on the VT persistence was tested in 3 hearts. The incidence of persisted (>30 seconds)/all VTs was 11 of 23 (48%) in control subjects, 1 of 26 (4%) during RC, and 8 of 13 (62%) 5 to 20 minutes after removal of the cooling device.

Optical images of excitation were analyzed in 5 hearts (9 VTs before RC and 13 VTs during RC) exhibiting visible rotor(s). In control, the rotors were, in most cases (7 of 9) stable with small meandering. The 13 VTs induced during RC, in contrast, were all unstable with remarkable meandering of rotors along the periphery of the RC region, and they terminated shortly. Action potential traces revealed frequent intermittent conduction block in the RC region with longer APD, giving rise to drift of the reentry circuit (Online Supplementary Figure 1). The rotors terminated by collision with anatomical boundaries in 7 VTs (Online Supplementary Figure 1), whereas by mutual annihilation in the RC region in 2 cases (Online Supplementary Figure 2). The mode of rotor termination was unable to be analyzed in the remaining 4 cases.

Termination of sustained VT by RC

We next examined the effects of RC applied during sustained VTs (lasting >120 seconds). We induced 76 sustained VTs in 15 hearts and observed them for 30 seconds with and without RC (33 VTs with RC, and 43 VTs without RC as control subjects). None of the 43 sustained VTs terminated in control subjects, whereas 16 of 33 (48%) sustained VTs terminated during the observation period with RC. Average time to termination was 12.5 ± 5.1 seconds (n = 16).

Optical images of excitation were analyzed in 16 sustained VTs that terminated during the RC application in 8 hearts. Figure 2 shows a representative experiment. Before the RC application, a stable clockwise rotor circulated around a functional block line (FBL) (approximately 5.1 mm); the bipolar electrogram showed a monomorphic pattern (Figure 2A, and Online Supplementary Video 1). A 3-D plot of the phase singularity (PS) trajectory obtained after phase mapping confirmed the stationarity of the rotor activity. Application of RC resulted in a dramatic change of the rotor dynamics and the VT terminated after approximately 10 seconds. Figure 2B shows isochrone maps during the last 3 beats prior to VT termination. A clockwise rotor circulated around a very long and curved FBL in the RC region in beat 1 and 2. The FBL configuration changed beat to beat in such a way that during beat 3 the FBL extended from the RC region to the atrioventricular groove, resulting in termination of reentry. The bipolar electrogram showed a polymorphic pattern before termination. Action potentials (Figure 2C) from the RC region (d) were longer compared with those outside (a–c, e, f), and this provided a substrate for conduction block. In Figure 2D, phase maps (left) and a 3-D plot of the PS trajectory (right) demonstrated that a single PS moved along the periphery of the RC region and collided with the atrioventricular groove (Online Supplementary Video 2). The mode of rotor termination by RC could be analyzed in 6 sustained VTs. In 4 sustained VTs, rotor terminated by drift and subsequent collision of PSs with boundaries, whereas in the remaining 2 cases, by mutual annihilation of PSs with opposite chiralities in the RC region.

RC failed to terminate 17 of 33 (52%) of the sustained VTs. The failure was attributable in part to the topological relationship between the rotor and the RC region. In other words, the success rate of RC cardioversion was relatively high (12 of 19) when the rotation center was located within or in the vicinity of the RC region. However, success was low (4 of 14) when the rotation center was far from the RC region.

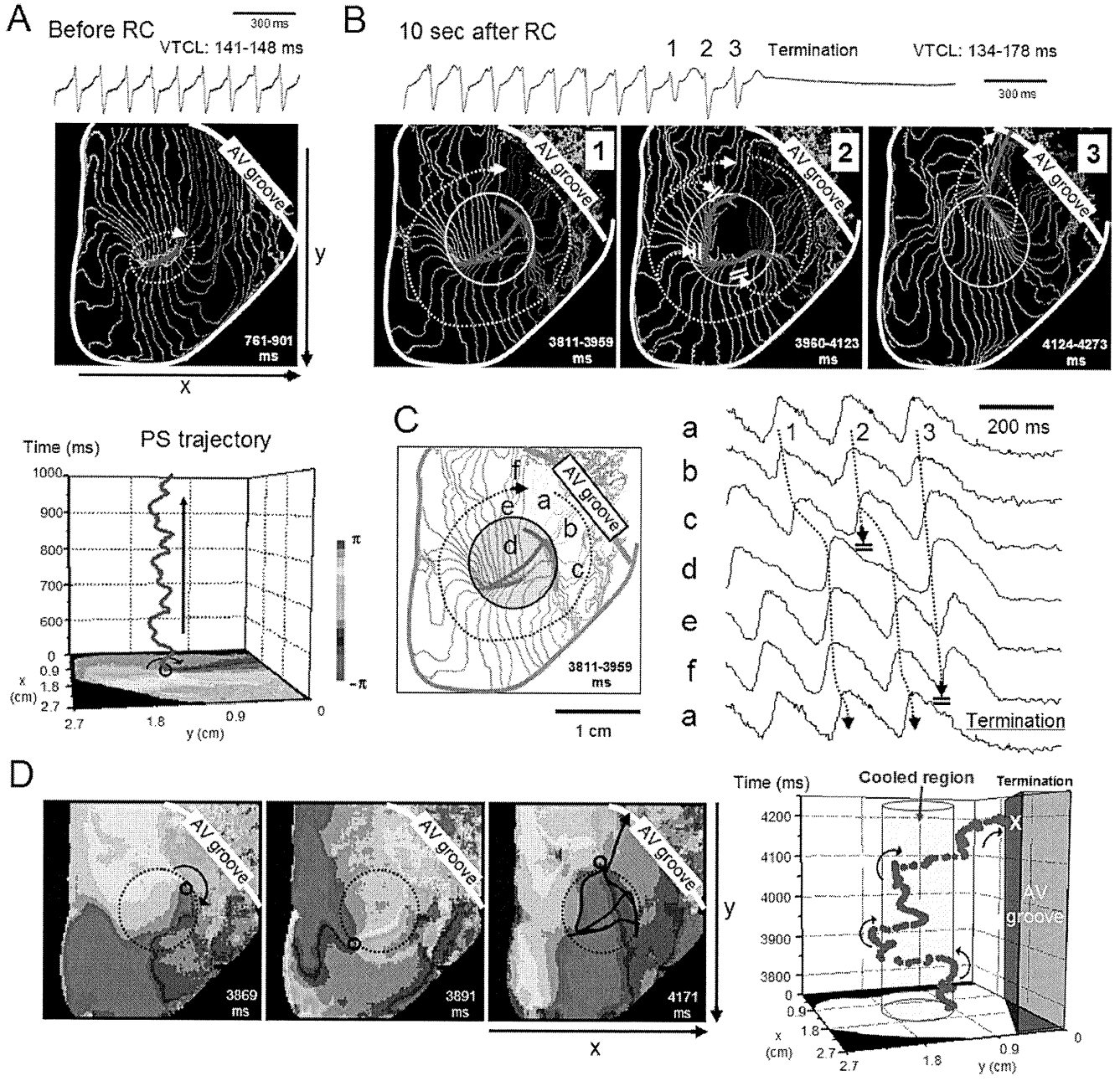

Figure 2 Termination of sustained VT by RC. **A:** Bipolar electrogram (top) and 4-ms isochrone map (middle) of sustained VT (>120 seconds) before RC application. Bottom, trajectory of a PS plotted on space-time axes. Stable reentrant activity was maintained. **B:** Bipolar electrogram (top) and isochrone maps (bottom) of 3 consecutive beats prior to VT termination approximately 10 seconds after RC. A clockwise rotor rotating around a long and curved FBL (pink) changed circuits in each excitation. Yellow circle, RC region. **C:** Optical action potential signals (a–f in the isochrone map) prior to VT termination. Wave propagation was frequently blocked at the periphery of the RC region. **D:** Left, phase maps of the last 2 beats. Black circle, PS of clockwise rotation; dotted circle, RC region. Right, PS trajectory plotted on space-time axes. Blue column, RC region. PS = phase singularity; VT = ventricular tachycardia; other abbreviations as in Figure 1.

Cardioversion of sustained VT by DC shock

When the sustained VTs did not terminate during the 30-second observation period, DC cardioversion was attempted. DC shocks of 15 to 80 V were applied to 21 sustained VTs in the absence of RC (in 12 hearts) and 16 sustained VTs in presence of RC (in 9 hearts) to evaluate the threshold DC shock intensity for cardioversion. The threshold DC shock intensity required for VT termination was significantly less with RC (22.8 ± 4.1 V, n = 16) than that without RC (40.5 ± 17.6 V, n = 21, $P < .05$).

The mode of rotor modification and termination by DC shocks with and without RC was also different. Representative experiments are shown in Figure 3. Figure 3A is the consequence of a 25-V shock that failed to terminate the reentrant activity in the absence of RC. A single clockwise rotor (PS1) was present before the DC shock; shock appli-

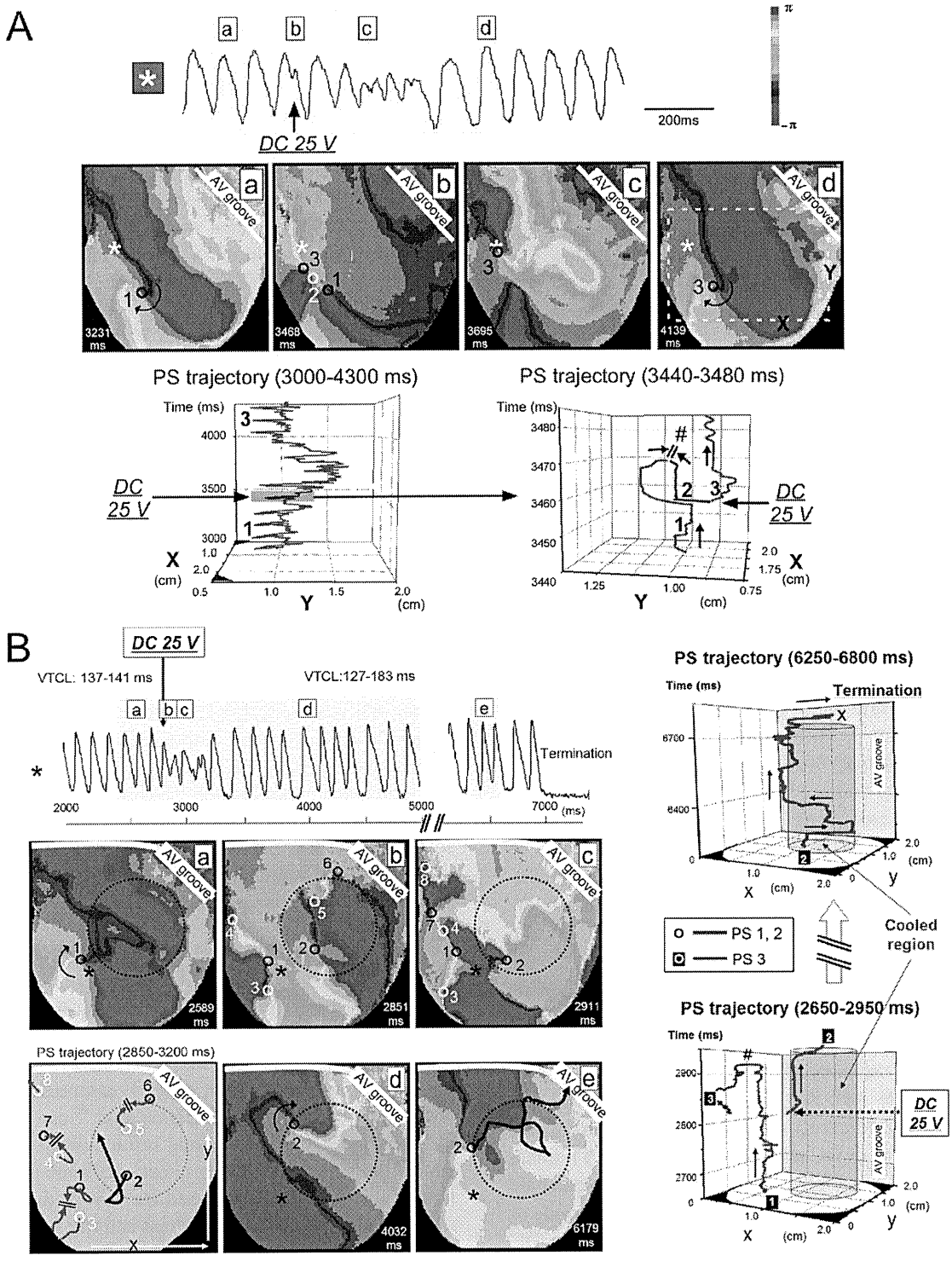

Figure 3 Rotor modification by DC shock applied to sustained VT in the absence and presence of RC. **A:** Failure of cardioversion by low-intensity shock in the absence of RC through repining of PS. Top, action potential trace; middle, phase maps before and after 25-V DC shock application. Black and white circles, PSs of clockwise and counterclockwise rotation, respectively. *Site of action potential recording. Bottom, trajectory of PSs plotted on space-time axes. A part of the trajectory in the left panel (immediately before and after DC shock application) is expanded in the right panel to show generation, mutual annihilation (#), and repining of PSs. **B:** Success of cardioversion by low-intensity DC shock in the presence of RC through unpinning of PS. Left, action potential trace (top) and phase maps (bottom) before (a) and after application of a 25-V DC shock (b–e). The shock application generated new PSs (black and white circles, clockwise and counterclockwise rotation, respectively). Trajectory of the PSs is illustrated in the right bottom panel. PS8 was pushed out of the observation area after meandering. PS1-PS3, PS4-PS7, and PS5-PS6 dissipated by mutual annihilation within 100 ms. PS2 survived and drifted in the periphery of the RC region (unpinning), and collided with the atrioventricular groove. *Site of action potential recording. Right, trajectory of PSs 1-3 plotted on space-time axes. Blue columns indicate the RC region. Abbreviations as in Figure 2.

cation generated a pair of PSs (counterclockwise PS2 and clockwise PS3). Then, PS1 and PS2 collided with each other and disappeared, whereas PS3 survived by anchoring and subsequently maintained the reentrant activity. Thus, as confirmed by the 3-D PS trajectory plots, the rotor dynamics were destabilized transiently by the DC shock, but restabilized after PS repining. In this heart, application of a 30-V DC shock resulted in generation of multiple PSs exhibiting irregular meandering, and the activation pattern was transformed from VT to VF (Online Supplementary Figure 3A), and application of a high-voltage (50 V) DC shock resulted in a prompt disappearance of reentrant activities by shock-induced phase resetting (Online Supplementary Figure 3B).

Figure 3B is the consequence of a 25-V DC shock, which terminated the reentrant activity in the presence of RC. Before the shock, a single clockwise rotor (PS1) anchored to a site close to the RC region (left, a). DC shock at 25 V created 7 new PSs (PSs2 to 8) of either chirality that meandered following complex trajectories (b and c). Then, PS1-PS3, PS4-PS7, and PS5-PS6 disappeared by mutual annihilation. PS8 moved out of the left margin (toward the posterior surface). PS2 survived and drifted along the periphery of the RC region (d and e). The VT terminated by collision of PS2 with the atrioventricular groove approximately 4 seconds after the DC shock application (top). Figure 3B, right, illustrates the trajectory of PSs plotted on space-time axes.

Figure 4 summarizes the data obtained from 18 sustained VTs (in 12 hearts) without RC and 13 sustained VTs (in 9 hearts) with RC exhibiting visible rotors; 38 and 17 DC shocks were applied without and with RC, respectively. In the cases of cardioversion failure, the mode of SW modification was classified into 3 types: no substantial change, repining of rotors (see Figure 3A), and transformation from VT to VF (see Online Supplementary Figure 3A). In the case of cardioversion success, the mode of SW modification was classified into 2 forms; unpinning of rotors followed by collision and extinction (see Figure 3B), and immediate disappearance of rotors by phase resetting (see Online Supplementary Figure 3B). As shown in Figure 4A, for DC shocks without RC (control), the major mode of success was phase resetting at high DC shock intensities (≥50 V); transformation from VT to VF often occurred at intermediate intensities (30 to 40 V), and repining was the major mode of failure at relatively low intensities (20 to 30 V). For DC shocks with RC, in contrast, the major mode of success was unpinning with relatively low intensities (15 to 25 V), and the major mode of failure was no change. Figure 4B compares the success rate of DC cardioversion with and without RC. The intensity-response curve with RC was shifted to the left from that without RC (control) by 17.7 V. Average time to VT termination tended to be longer in the presence of RC (1.6 ± 1.9 seconds, n = 13) compared with that in the absence of RC (0.6 ± 1.2 seconds, n = 18), although the difference remained statistically insignificant (Figure 4C).

Effects of RC on VT/VF induced in 3-D hearts

We examined the effects of RC on the sustained VT/VFs (>120 seconds) in 6 intact hearts without cryoablation. A total of 17 sustained VT/VFs were induced. In 8 control VT/VFs, in which RC was not imposed, all (8 of 8) continued during the 30-second observation period. Subsequent application of biphasic DC shocks terminated 3 of 8 VT/VFs. In 9 VT/VFs, in which RC cardioversion was attempted, 1 of 9 terminated within 30 seconds by RC alone; subsequent application of DC shocks in the presence of RC terminated 7 of 8 VT/VFs. The threshold amplitude for the DC cardioversion was 56.7 ± 5.8 V (n = 3) in the absence of RC (control), and 31.4 ± 8.5 V (n = 7) in the presence of RC (P <.05). Time for cardioversion after DC application was 1.3 ± 1.7 seconds (n = 3) in the absence of RC and 12.2 ± 11.2 seconds (n = 7) in the presence of RC (P <.05). DC shocks at the maximum voltage (100 V) failed to terminate 5 of 8 VT/VFs in the absence of RC, but 1 of 8 in the presence of RC. Thus, RC facilitated cardioversion in 3-D hearts when combined with DC shocks in association with a certain modification of the mode of reentry termination.

Discussion

The major findings in the present study are as follows. First, rotors induced during RC were initially confined to the RC region, but were unstable and terminated early by collision following drift. Second, rotors underlying sustained VTs were transformed by RC from stationary to nonstationary; RC terminated approximately 50% of sustained VTs. Third, the threshold intensity of DC shocks for cardioversion of sustained VTs was reduced in the presence of RC; the major mode of rotor termination by DC shocks was changed from phase resetting to unpinning.

RC destabilizes rotors in favor of their termination

In the experiments in which VTs were induced during RC (the first protocol), 98% of the VTs self-terminated within 5 seconds because the rotors were unstable and drifted around the RC region. This finding, which is essentially concordant with a previous report by Boersma et al,[18] can be explained by creation of a region of long refractoriness and reduced conductivity by RC. During constant stimulation, RC prolonged the APD and decreased the CV in the RC region, which explained why the reentrant activity was impaired in the RC region, and was accompanied by intermittent conduction block and long tortuous PS meandering trajectories in the periphery of the RC region. We have previously demonstrated that global myocardial cooling (30°C to 33°C) caused an increase of the maximum APD restitution slope and a broadening of CV restitution curves compared with control subjects.[17] These changes of the restitution properties would increase destabilization of the reentry in the RC region through an enhancement of wavefront-tail interactions.[17] Temperature-dependent alterations of electrotonic effects, short-term memory, and perhaps intracellular Ca^{2+}

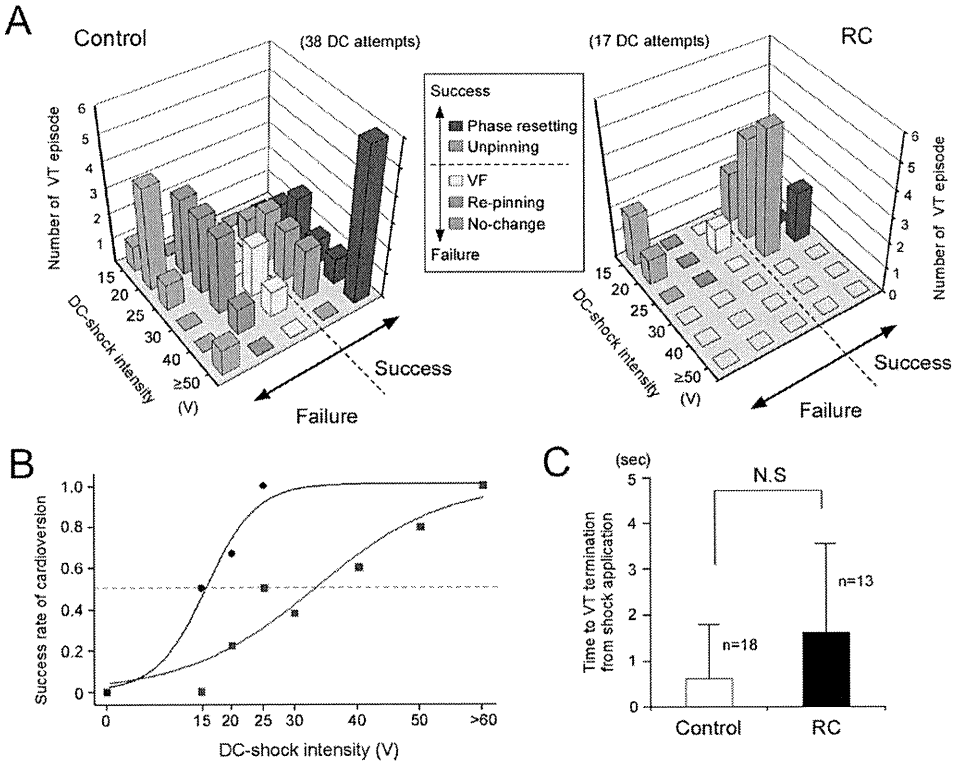

Figure 4 Modification of rotor dynamics by DC shocks applied to sustained VT. **A:** Intensity-dependent modification of rotor dynamics by DC shocks in the absence (control) and presence of RC. In the case of cardioversion success, the rotor modification was either phase resetting (red) or unpinning of PSs followed by collision and extinction (orange). When the cardioversion was failed, the rotor modification was either no substantial change (blue), repining of PSs (green) or transformation from VT to VF (yellow). **B:** Intensity-response of the success rate of DC cardioversion without (control, red) and with RC (blue). The shock intensity for 50% success was 33.3 V without RC (38 VTs) and 15.5 V with RC (18 VTs). **C:** Time required for VT termination from the instant of shock application without RC (control, n = 18) and with RC (n = 13, not significant). Abbreviations as in Figure 2.

dynamics might also contribute to rotor destabilization,[9] but such factors remain to be elucidated.

Mathematical model analysis of the rotor dynamics has demonstrated that spatial gradients in refractoriness play important roles in the stability of the rotation center in the cardiac muscle with normal excitability.[21–23] In a medium with stepwise heterogeneity, rotors move along the border separating regions with different refractoriness.[21] Our observation showing enormous PS drift in the periphery of the RC region is consistent with theoretical prediction.

To assess the potential usefulness of RC for cardioversion, we investigated the effects of RC on sustained VTs and found that RC terminated approximately 50% of sustained VTs. In the cases of successful cardioversion, the rotor dynamics changed dramatically from stationary to nonstationary. The nonstationary rotors shared common features with those induced after RC application in terms of long tortuous FBLs confined to the RC region and tremendous drift of rotors leading to their collision and extinction. The effects of RC on VT perpetuation were reversible upon removal of RC, suggesting a potential advantage of RC as a therapeutic procedure. The failure of RC cardioversion was attributable partly to the topological relationship between the pre-existing rotor and the RC region; when the rotation center was outside the RC region, the success rate of cardioversion was low. The RC cardioversion also depends on the size of the cooling area. In our pilot experiments, we tested the effects of RC to reduce the temperature by approximately 6°C from the baseline (36°C) in a circular area of 3 different size (5, 8, and 10 mm in diameter). Sustained VTs were terminated efficiently (16 of 33 VTs, 48%) by RC alone only with the largest size tested.

RC reduces the DC shock intensity required for cardioversion

When RC failed to terminate sustained VTs, we attempted DC cardioversion in the presence of RC. Those VTs were likely to be maintained by stationary rotors with PSs anchored at structural discontinuities. Our experiments showed that application of relatively low-intensity DC shocks always created new multiple PSs, resulting from shock-induced virtual electrode polarization.[24] SW reentry can be induced by a combination of depolarization and hyperpolarization at a close proximity.[24,25]

In control subjects (without RC), relatively weak DC shocks caused displacement of preexisting PSs (unpinning) and generated new PSs. Eventually such new PSs disappeared, but organized stationary SW reentry was resumed when the survived PSs were anchored again. Another mode of cardioversion failure was transformation from VT to VF, which was the result of irregular meandering of multiple, widely dispersed PSs. The major mode of cardioversion success in control subjects was immediate PS disappearance by phase resetting at intensities larger than the upper limit of vulnerability.[26] In contrast, when DC shocks of weak intensities were applied in the presence of RC, unpinning of PSs was not followed by repining. Instead, PSs drifted along the periphery of the RC region, eventually colliding and disappearing. Thus, the major mode of cardioversion success in the presence of RC was unpinning. The threshold shock

intensity was reduced significantly (by approximately 50%) from control subjects. Transformation from VT to VF rarely occurred in the presence of RC. These results suggest that RC facilitates DC cardioversion by confining and destabilizing rotors in the RC region.

Ripplinger et al[16] demonstrated in isolated rabbit right ventricular preparations that unpinning and destabilization of rotors leading to VT termination can be induced by weak DC shocks, provided that shocks are applied at a certain phase of the VT cycle.[16,22] A greater reduction of the DC shock intensity might be possible for cardioversion in combination with RC if the shocks were applied at a restricted phase. Further experimental studies are required to address the issue.

Study limitations

We showed facilitation of VT termination by RC in 2-D ventricular myocardium of rabbit hearts through unpinning and collision of rotors. We used BDM, which is known to affect ion channels and intracellular Ca^{2+} dynamics and to reduce muscle contraction. However, this does not seem to invalidate our results, because characteristic modification of rotor dynamics by RC was preserved in the absence of BDM (Online Supplementary Figure 5). Extrapolation of our observations in 2-D tissue preparations to 3-D and larger hearts is not straightforward. The chance of collision of rotors with boundaries would be reduced, and wave breakup would be enhanced in a larger 3-D tissue mass. In our experiments using intact 3-D rabbit hearts, in fact, RC alone was not effective for self-termination of sustained VT/VFs. However, the threshold intensity of DC shocks for cardioversion was significantly reduced in the presence of RC, and this was associated with an increase in the time required for cardioversion after the shock, suggesting alterations in the mode of reentry termination. Accordingly, a certain benefit of RC favoring low-energy defibrillation is considered to be preserved in 3-D hearts. Structural discontinuities and functional heterogeneities would alter the requirements for rotor termination. In addition, focal activities may also play roles in VT/VF.[27] To the best of our knowledge, there are no efficient RC devices applicable to clinical practice, and this is a critical issue to be solved in the future. Despite these limitations, the present study provides a new perspective toward the development of low-energy cardioversion/defibrillation.

Appendix

Supplementary data

Supplementary data associated with this article can be found, in the online version, at doi:10.1016/j.hrthm.2011.08.013.

References

1. Buxton AE, Lee KL, Fisher JD, Josephson ME, Prystowsky EN, Hafley G. A randomized study of the prevention of sudden death in patients with coronary artery disease. Multicenter Unsustained Tachycardia Trial Investigators. N Engl J Med 1999;341:1882–1890.
2. Lee DS, Green LD, Liu PP, et al. Effectiveness of implantable defibrillators for preventing arrhythmic events and death: a meta-analysis. J Am Coll Cardiol 2003;41:1573–1582.
3. Weaver WD, Cobb LA, Copass MK, Hallstrom AP. Ventricular defibrillation: a comparative trial using 175-J and 320-J shocks. N Engl J Med 1982;307:1101–1106.
4. Waldecker B, Brugada P, Zehender M, Stevenson W, Wellens HJ. Dysrhythmias after direct-current cardioversion. Am J Cardiol 1986;57:120–123.
5. Runsiö M, Kallner A, Källner G, Rosenqvist M, Bergfeldt L. Myocardial injury after electrical therapy for cardiac arrhythmias assessed by troponin-T release. Am J Cardiol 1997;79:1241–1245.
6. Godemann F, Butter C, Lampe F, et al. Panic disorders and agoraphobia: side effects of treatment with an implantable cardioverter/defibrillator. Clin Cardiol 2004;27:321–326.
7. Kamphuis HC, Verhoeven NW, Leeuw R, Derksen R, Hauer RN, Winnubst JA. ICD: a qualitative study of patient experience the first year after implantation. J Clin Nurs 2004;13:1008–1016.
8. Jalife J. Ventricular fibrillation: mechanisms of initiation and maintenance. Annu Rev Physiol 2000;62:25–50.
9. Weiss JN, Qu Z, Chen PS, et al. The dynamics of cardiac fibrillation. Circulation 2005;112:1232–1240.
10. Biktashev VN, Holden AV. Design principles of a low voltage cardiac defibrillator based on the effect of feedback resonant drift. J Theor Biol 1994;169:101–112.
11. Morgan SW, Plank G, Biktasheva IV, Biktashev VN. Low energy defibrillation in human cardiac tissue: a simulation study. Biophys J 2009;96:1364–1373.
12. Garfinkel A, Spano ML, Ditto WL, Weiss JN. Controlling cardiac chaos. Science 1992;257:1230–1235.
13. Pak HN, Liu YB, Hayashi H, et al. Synchronization of ventricular fibrillation with real-time feedback pacing: implication to low-energy defibrillation. Am J Physiol Heart Circ Physiol 2003;285:H2704–H2711.
14. Pak HN, Okuyama Y, Oh YS, et al. Improvement of defibrillation efficacy with preshock synchronized pacing. J Cardiovasc Electrophysiol 2004;15:581–587.
15. Ripplinger CM, Krinsky VI, Nikolski VP, Efimov IR. Mechanisms of unpinning and termination of ventricular tachycardia. Am J Physiol Heart Circ Physiol 2006;291:H184–H192.
16. Li W, Ripplinger CM, Lou Q, Efimov IR. Multiple monophasic shocks improve electrotherapy of ventricular tachycardia in a rabbit model of chronic infarction. Heart Rhythm 2009;6:1020–1027.
17. Harada M, Honjo H, Yamazaki M, et al. Moderate hypothermia increases the chance of spiral wave collision in favor of self-termination of ventricular tachycardia/fibrillation. Am J Physiol Heart Circ Physiol 2008;294:H1896–H1905.
18. Boersma L, Zetelaki Z, Brugada J, Allessie M. Polymorphic reentrant ventricular tachycardia in the isolated rabbit heart studied by high-density mapping. Circulation 2002;105:3053–3061.
19. Yamazaki M, Honjo H, Nakagawa H, et al. Mechanisms of destabilization and early termination of spiral wave reentry in the ventricle by a class III antiarrhythmic agent, nifekalant. Am J Physiol Heart Circ Physiol 2007;292:H539–H548.
20. Ishiguro YS, Honjo H, Opthof T, et al. Early termination of spiral wave reentry by combined blockade of Na^+ and L-type Ca^{2+} currents in a perfused two-dimensional epicardial layer of rabbit ventricular myocardium. Heart Rhythm 2009;6:684–692.
21. Fast VG, Kléber AG. Role of wavefront curvature in propagation of cardiac impulse. Cardiovasc Res 1997;33:258–271.
22. Fast VG, Rohr S, Gillis AM, Kléber AG. Activation of cardiac tissue by extracellular electrical shocks: formation of 'secondary sources' at intercellular clefts in monolayers of cultured myocytes. Circ Res 1998;82:375–385.
23. Kléber AG, Rudy Y. Basic mechanisms of cardiac impulse propagation and associated arrhythmias. Physiol Rev 2004;84:431–488.
24. Efimov IR, Cheng Y, Van Wagoner DR, Mazgalev T, Tchou PJ. Virtual electrode-induced phase singularity: a basic mechanism of defibrillation failure. Circ Res 1998;82:918–925.
25. Trayanova NA, Gray RA, Bourn DW, Eason JC. Virtual electrode-induced positive and negative graded responses: new insights into fibrillation induction and defibrillation. J Cardiovasc Electrophysiol 2003;14:756–763.
26. Gray RA, Chattipakorn N. Termination of spiral waves during cardiac fibrillation via shock-induced phase resetting. Proc Natl Acad Sci USA 2005;102:4672–4677.
27. Tabereaux PB, Dosdall DJ, Ideker RE. Mechanisms of VF maintenance: wandering wavelets, mother rotors, or foci. Heart Rhythm 2009;6:405–415.

Images and Case Reports in Arrhythmia and Electrophysiology

Successful Catheter Ablation of Bidirectional Ventricular Premature Contractions Triggering Ventricular Fibrillation in Catecholaminergic Polymorphic Ventricular Tachycardia With *RyR2* Mutation

Takashi Kaneshiro, MD; Yoshihisa Naruse, MD; Akihiko Nogami, MD; Hiroshi Tada, MD; Kentaro Yoshida, MD; Yukio Sekiguchi, MD; Nobuyuki Murakoshi, MD; Yoshiaki Kato, MD; Hitoshi Horigome, MD; Mihoko Kawamura, MD; Minoru Horie, MD; Kazutaka Aonuma, MD

The subject of this report is a 38-year-old woman who often experienced syncope since childhood. Syncope occurred >10 times a year and was associated with convulsion during exercise and emotionally exciting situations. The patient's 13-year-old daughter had also experienced frequent episodes of syncope and developed ventricular fibrillation (VF) during treadmill exercise testing that was successfully defibrillated with electric shock. Witnessing this situation, the patient also lost consciousness, with documented VF that was converted to sinus rhythm by cardiopulmonary resuscitation without electric defibrillation.

Both the patient and her daughter were admitted to our hospital. We performed echocardiography, coronary angiography, and cardiac CT, the results of which revealed no structural heart disease. Resting 12-lead ECG did not indicate any abnormalities, including long-QT syndrome or Brugada syndrome. A signal-averaged ECG revealed no late potentials. Treadmill exercise testing easily induced bigeminal ventricular premature contractions (VPCs) with a right bundle branch block configuration and inferior axis (Figure 1A), and the exercise was terminated because of intolerable symptoms. Catecholamine stress test was started with administration of continuous intravenous infusion of epinephrine in a stepwise manner from 0.025 μg/kg per minute.[1] During epinephrine infusion at a rate of 0.1 μg/kg per minute, multifocal VPCs (VPC #1, right bundle branch block configuration and superior axis; VPC #2, right bundle branch block configuration and inferior axis [the same VPC configuration as that induced during the treadmill exercise testing]; and VPC #3, left bundle branch block configuration and inferior axis) appeared, and VPC #1 following VPC #2 subsequently induced VF (Figure 1B).

Administration of bisoprolol 5 mg QD was given but failed to suppress the exercise-induced bigeminal VPCs with the same morphology as induced previously. Because frequent deliveries of shock were believed to be likely, even with β-blocker treatment, catheter ablation was offered to the patient before implantable cardioverter-defibrillator (ICD) implantation. Catheter mapping and ablation for the bidirectional VPCs were performed with a 3D electroanatomic mapping system (CARTO; Biosense Webster) and a 3.5-mm-tip irrigation catheter (NaviStar; Thermo Cool) with only local anesthesia. No VPCs, ventricular tachycardia (VT), or VF were inducible with burst pacing and programmed stimulation from both right ventricular apex and right outflow tract during baseline and continuous intravenous infusion of isoproterenol.

With epinephrine infusion at a rate of 0.1 μg/kg per minute, VPC #1 and VPC #2 appeared. VPC #1 was nonsustained, and a presystolic Purkinje potential was recorded at the left ventricular inferoseptal area near the posteromedial papillary muscle, which preceded the onset of VPC #1 by 18 ms. The unipolar electrogram from the ablation catheter during VPC #1 showed a QS pattern, and a perfect match of the QRS configuration was obtained by pace mapping (Figure 2). Radiofrequency energy application to this site provoked some ventricular acceleration beats, and several radiofrequency energy applications around the target site finally eliminated all the VPCs, resulting in complete suppression of all VPC #1.

After the ablation of VPC #1, isolated occurrences of VPC #2 continued, and a local bipolar electrogram recorded on the left coronary cusp showed discrete prepotential that preceded the onset of VPC #2 by 65 ms, and a perfect match of the

Received July 26, 2011; accepted January 5, 2012.

From the Cardiovascular Division, Institute of Clinical Medicine (T.K., Y.N., H.T., K.Y., Y.S., N.M., K.A.) and Department of Child Health (Y.K., H.H.), Graduate School of Comprehensive Human Sciences, University of Tsukuba, Tsukuba, Japan; Division of Heart Rhythm Management, Yokohama Rosai Hospital, Yokohama, Japan (A.N.); and Department of Cardiovascular and Respiratory Medicine, Shiga University of Medical Science, Shiga, Japan (M.K., M.H.).

Correspondence to Kazutaka Aonuma, MD, Cardiovascular Division, Institute of Clinical Medicine, Graduate School of Comprehensive Human Sciences, University of Tsukuba, 1-1-1 Tennodai, Tsukuba, Ibaraki 305-8575, Japan. E-mail kaonuma@md.tsukuba.ac.jp

(*Circ Arrhythm Electrophysiol.* **2012;5:e14-e17.**)

Circ Arrhythm Electrophysiol **is available at http://circep.ahajournals.org** **DOI: 10.1161/CIRCEP.111.966549**

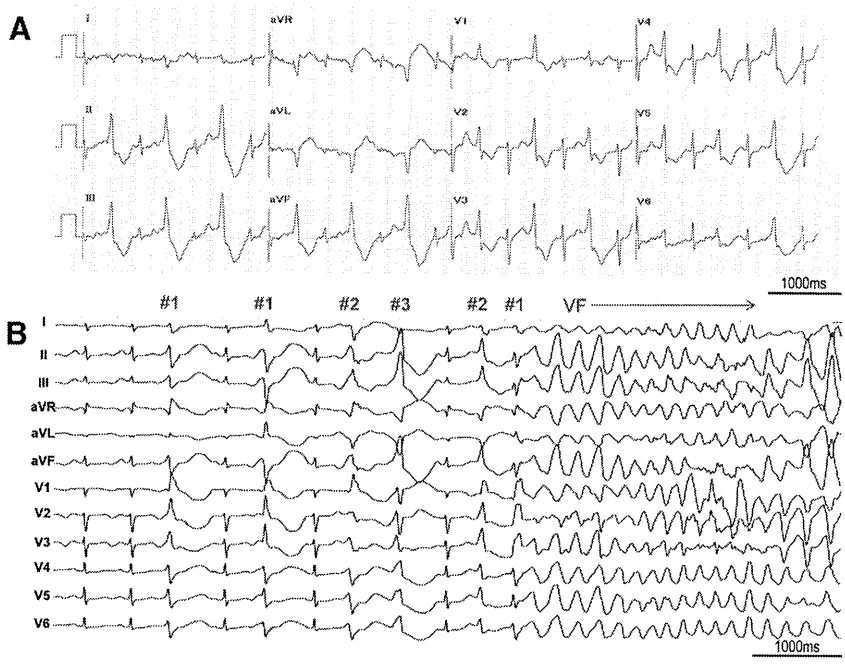

Figure 1. A, Twelve-lead ECG recording during treadmill exercise testing. Bigeminal ventricular premature contractions (VPCs) appeared during the second stage of the Bruce protocol. VPC morphology represented a right bundle branch block configuration and inferior axis. Because the patient experienced intolerable symptoms, the test was discontinued. **B**, Epinephrine stress test. Continuous intravenous infusion of epinephrine was started from a rate of 0.025 μg/kg per minute, and the QT interval did not changed. At a rate of 0.1 μg/kg per minute, VPC #1 (right bundle branch block configuration and superior axis), VPC #2 (right bundle branch block configuration and inferior axis, same as that induced in the treadmill exercise testing), and VPC #3 (left bundle branch block configuration and inferior axis) were induced. Subsequently, VPC #1 following VPC #2 suddenly induced ventricular fibrillation, which was successfully terminated with electric shock.

QRS configuration was obtained by pace mapping (Figure 3). Radiofrequency energy application to the left coronary cusp abolished VPC #2 4 s after the onset of radiofrequency energy application. After successful catheter ablation of bidirectional VPCs, neither VPCs nor VF were inducible, even with an infusion of epinephrine of up to 1.2 μg/kg per minute (a >10 times higher dose than provocation). Precise ablation sites in a 3D electroanatomic mapping merged with contrast-enhanced CT are shown in Figure 4.

ICD implantation was performed, and the patient was discharged from the hospital on bisoprolol 2.5 mg QD. Serial Holter ECGs after the ablation showed only 3 to 5 isolated VPCs with a different morphology from the previously observed VPCs, and treadmill exercise testing induced no VPCs at the maximal workload. During 16-month follow-up, neither episodes of syncope nor ICD therapy occurred. Genetic analysis revealed a mutation in the ryanodine receptor gene (*RyR2*), and a diagnosis of catecholaminergic polymorphic VT (CPVT) was confirmed (Figure 5).[2] The patient's daughter was also given a diagnosis of CPVT with same mutation in *RyR2* and had catheter ablation for the origins of bidirectional VT. Although she refused ICD

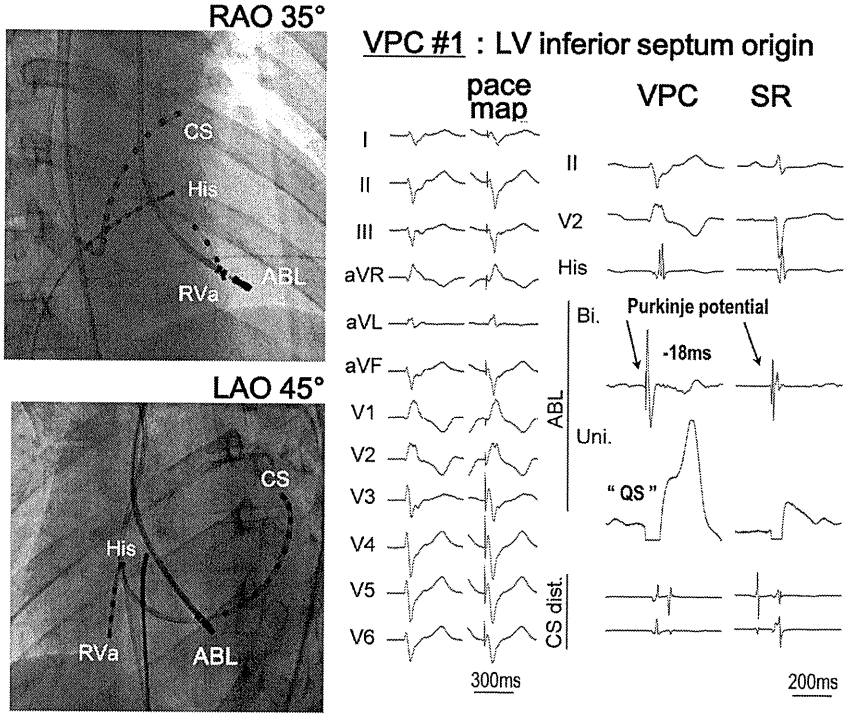

Figure 2. Activation mapping and pace mapping for VPC #1. A Purkinje potential was recorded from the left ventricular inferoseptum and preceded the QRS onset by 18 ms. The unipolar electrogram recorded from the distal electrode showed a QS pattern. Perfect pace mapping was obtained at this site. ABL indicates ablation catheter; CS, coronary sinus; His, His bundle; LAO, left anterior oblique; RAO, right anterior oblique; RVa, right ventricular apex; SR, sinus rhythm; VPC, ventricular premature contraction.

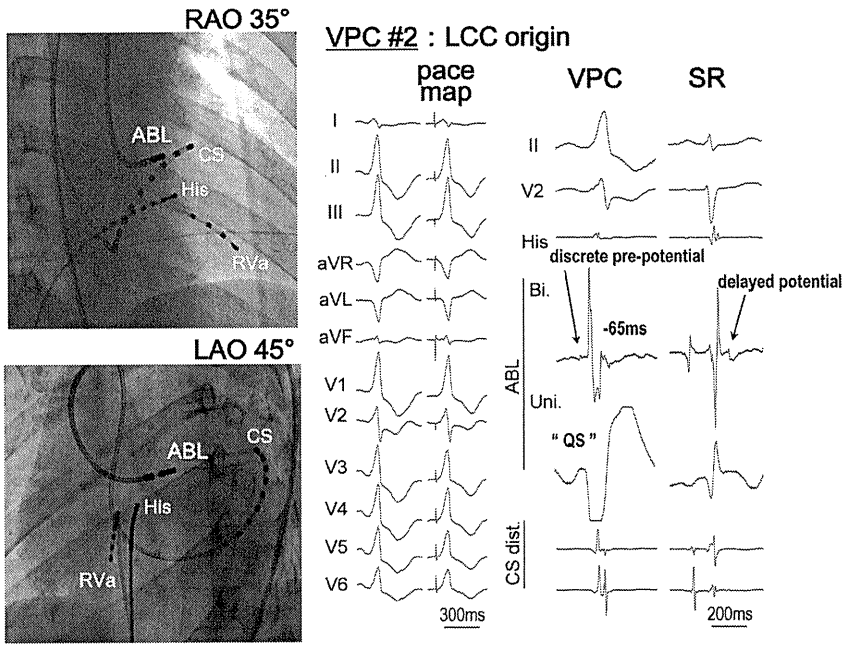

Figure 3. Activation mapping and pace mapping for VPC #2. A local bipolar electrogram recorded from the LCC showed a discrete prepotential that preceded the QRS onset by 65 ms associated with a QS pattern of unipolar electrogram. Perfect pace mapping was obtained at this site. ABL indicates ablation catheter; CS, coronary sinus; His, His bundle; LAO, left anterior oblique; LCC, left coronary cusp; RAO, right anterior oblique; RVa, right ventricular apex; SR, sinus rhythm; VPC, ventricular premature contraction.

implantation, she had not experienced any episode of VT or syncope with β-blocker treatment.

The generally accepted therapy for CPVT has been β-blockers,[3] and the additional administration of flecainide or verapamil to β-blockers has been reported to be effective; however, the effects of those drugs are not fully standardized. For medically refractory cases, sympathetic denervation is one of the alternative treatment options. The ICD is considered the definitive therapy for the prevention of sudden cardiac death; however, failure to prevent sudden cardiac death has been reported in several cases because ICD shock delivery might lead to catecholamine release, resulting in an electric storm.[4] This concern prompted the decision to attempt catheter ablation of VPCs triggering VF. Although several reports have described successful catheter ablation of VPCs triggering VF in some patients with structurally normal hearts, such as those with Brugada syndrome, long-QT syndrome, and idiopathic VF, successful catheter ablation of VPCs triggering VF in CPVT has not been reported. Cerrone and colleagues[5] reported that the mechanism of CPVT was due to the delayed afterdepolarization-induced triggered activity in a focal Purkinje network in a knock-in (*RyR2*) mouse. However, whether the Purkinje system is related to the mechanism of VF in CPVT or just trigger origin is still unknown.

To our knowledge, this is the first report of successful catheter ablation of the bidirectional VPCs that trigger VF, and this procedure could become one of the adjunctive

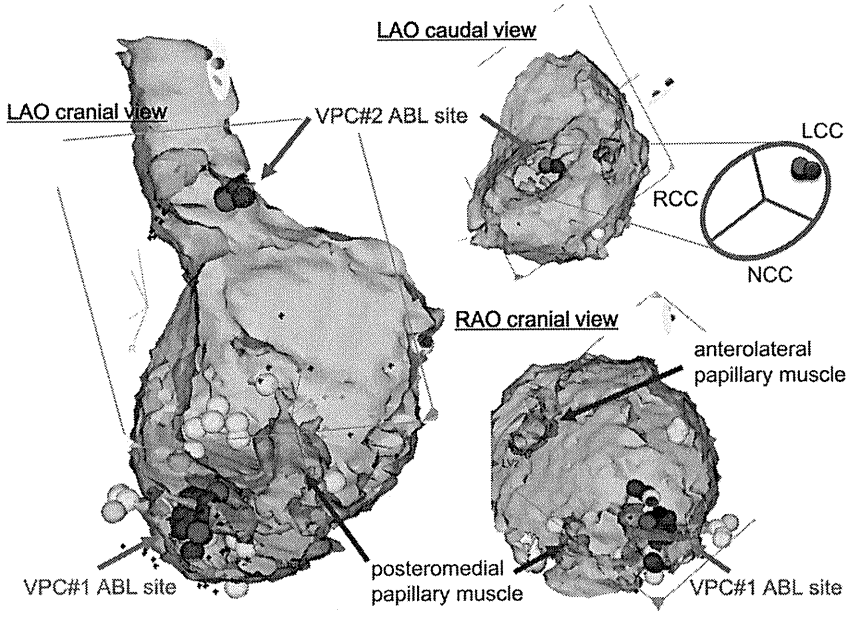

Figure 4. Electroanatomic mapping merged with contrast-enhanced CT. Red tags indicate the ABL sites. Blue tags indicate the sites with perfect pace mapping, and yellow tags indicate the sites with Purkinje potentials during sinus rhythm. The sites with perfect pace mapping and the earliest activation for VPC #1 were localized in the inferoseptal site adjacent to the base of the posteromedial papillary muscle (red arrow). Successful ablation site of VPC #2 was on the left coronary cusp (blue arrow). ABL indicates ablation; LAO, left anterior oblique; LCC, left coronary cusp; NCC, noncoronary cusp; RAO, right anterior oblique; RCC, right coronary cusp; VPC, ventricular premature contraction.